
Transfer Learning in Infinite Width Feature Learning Networks

Clarissa Lauditi¹, Blake Bordelon^{1,2}, Cengiz Pehlevan^{1,2}

¹ John A. Paulson School of Engineering and Applied Sciences

² Center for Brain Science & Kempner Institute for the Study of Natural and Artificial Intelligence

Harvard University

Cambridge, MA 02138

clauditi@seas.harvard.edu

blake_bordelon@g.harvard.edu

cpehlevan@seas.harvard.edu

Abstract

We develop a theory of transfer learning in infinitely wide neural networks where both the pretraining (source) and downstream (target) task can operate in a feature learning regime. We analyze both the Bayesian framework, where learning is described by a posterior distribution over the weights, and gradient flow training of randomly initialized networks trained with weight decay. Both settings track how representations evolve in both source and target tasks. The summary statistics of these theories are adapted feature kernels which, after transfer learning, depend on data and labels from both source and target tasks. Reuse of features during transfer learning is controlled by an elastic weight coupling which controls the reliance of the network on features learned during training on the source task. We apply our theory to linear and polynomial regression tasks as well as real datasets. Our theory and experiments reveal interesting interplays between elastic weight coupling, feature learning strength, dataset size, and source and target task alignment on the utility of transfer learning.

1 Introduction

Modern deep-learning models achieve remarkable accuracy by scaling parameters, computation, and data [1, 2, 3]. Yet collecting such large volumes of data is prohibitively expensive or outright impossible in many settings. Transfer learning offers a principled escape from this data bottleneck: by repurposing representations learned on data-rich source tasks, it reduces sample complexity while improving generalization [4, 5, 6, 7]. Therefore, understanding which properties of the pretraining and downstream data distributions enable effective transfer is critical for modern deep learning. Despite its empirical success, transfer learning still lacks a principled theory that predicts when it will succeed. In this paper, we present a novel theory of transfer learning in two-layer neural networks that elucidate the rich phenomenology of transfer learning.

Mathematically analyzing transfer learning is challenging, in part because representation learning in generic neural networks with realistic data remains poorly understood. To overcome this difficulty, we focus on transfer after **representation learning in infinite-width neural networks** in the μP /mean-field parameterization [8, 9, 10, 11]. In this parameterization, feature learning is preserved even as the width of the network goes to infinity. We focus on supervised learning for both source and target tasks and derive results for the network predictor after each phase of transfer learning. In particular, we analyze (1) Bayesian networks (building on the prior works [12, 13, 14]) and (2) transfer learning

through gradient flow. Our infinite width theory enables accurate predictions of the resulting network models for wide but finite neural networks.

Concretely, the contributions of this work are the following:

- We develop two different theoretical analyses of transfer learning for wide neural networks in the mean-field/ μP scaling, one based on a Bayesian formalism and the other on gradient flow dynamics with weight decay. These theories predict that NNs subject to transfer learning converge to adaptive kernel machines [14]. Here, the kernels depend both on the features learned from the specific (target) task \mathcal{T}_2 the model is trained on, and on the features transferred from a model pre-trained on a source task \mathcal{T}_1 .
- In our theories, hidden preactivations on target task \mathcal{T}_2 include both contributions from feature learning - tuned by a scalar hyperparameter γ_0 - and from transfer learning, which introduces a systematic shift towards the preactivation of the source model on target task \mathcal{T}_2 data. This dual modulation captures the non-trivial effect of newly learned and pre-trained representations.
- We investigate our theories on linear and polynomial target functions where task similarity can be directly controlled. Intuitively, our theories reveal that increased elastic weight coupling improves transfer learning the most when source and target tasks are similar. However, if there is sufficient data on the target task, then stronger feature learning on the target task can compensate for reduced elastic weight coupling.
- We then apply our theories to real computer vision datasets. By changing the classes of images the model is trained on, we can manipulate similarity between source and target tasks. Our theories accurately predict how generalization improves from transfer learning when target task sample size is small.

1.1 Related Works

Transfer Learning from Theory of General Linear Models Several works have studied how properties of a representation support generalization from few examples on a downstream task [15, 16, 17, 18, 19]. A general result is that the geometry of the neural representation (kernel-task alignment) controls the ability to learn a new supervised task from limited data [20]. However, these theories take as given the hidden representation structure prior to transfer and do not allow for representations to adapt during the learning of the downstream task.

Training Dynamics in Wide Networks Recent years have seen significant research on the learning dynamics of wide, randomly initialized neural networks. In standard / neural tangent parameterization, wide neural networks are described by kernel methods [21, 22, 23]. In this same parameterization, corrections to this limit at large but finite width reveal weak (perturbative) feature learning corrections to this limit, linearizing the dynamics of hidden representations around their static infinite width value [24]. Alternatively, other works have explored parameterizations that allow infinite width networks to learn features, known as mean-field or μP scaling, resulting in fundamentally nonlinear predictor dynamics. These works developed tools to study the representation learning dynamics during gradient descent training in infinite width neural networks, which require adoption of the mean-field/ μP scaling of network width [8, 9, 10, 11, 25, 26]. In this infinite limit, the dynamics for kernels cannot be linearized around the lazy learning solution (which we refer to as non-perturbative).

Learning in Wide Bayesian Networks In contrast to gradient descent training, some works have pursued theory of networks sampled from a Bayesian posterior, which can be interpreted as the long-time limit of Langevin dynamics (noisy gradient flow) with weight decay [27]. In the infinite width limit ($N \rightarrow \infty$) with Neural Tangent Kernel (NTK) parameterization and dataset size P held constant, networks converge to neural network Gaussian process (NNGP) models, which lacks representation learning [28]. Moving beyond this kernel limit, a statistical mechanics theory for deep Bayesian multilayer Perceptrons MLPs in NTK parameterization in the proportional limit $P, N \rightarrow \infty$ with $P/N = \alpha$ have revealed a *scale-renormalization effect* where the predictor $f(\mathbf{x})$ takes the form $f(\mathbf{x}) = \sum_{\mu\nu \in [P]} q(\alpha) \Phi(\mathbf{x}, \mathbf{x}_\mu) [q(\alpha) \Phi + \lambda \mathbf{I}]_{\mu\nu}^{-1} y(\mathbf{x}_\nu)$ where $[\Phi]_{\mu\nu} = \Phi(\mathbf{x}_\mu, \mathbf{x}_\nu)$ is the final layer’s feature kernel under the prior, λ is the regularization, $y(\mathbf{x}_\mu)$ are the targets, and the scale factor $q(\alpha)$ is determined self consistently as a function of $\alpha = P/N$, the kernel gram matrix Φ

and the targets \mathbf{y} [29, 30, 31]. We note that the kernel governing the predictor in this theory does not exhibit any change in the relative size of the entries. This same theory, when applied to gated networks or convolutional networks, is described by a gate \times gate [32] or space \times space [33] matrix $Q_{s,s'}(\alpha)$. In this case, the entries within each block (each gate or spatial location) of this kernel only change through a scale constant $Q_{s,s}(\alpha)$, but some blocks are rescaled relative to other blocks. More recent works study Bayesian networks in NTK parameterization in this limit using tools from large deviation theory, which reveal that kernels can adapt more significantly in structure even in MLPs [13, 34, 35, 36]. In principle, the proportional limit in this large deviation setting requires computing second and third order derivatives of the mean field action. An alternative strategy that has also been explored in recent works is to *adopt a mean-field/ μP -like* parameterizations where even the $N \rightarrow \infty$ limit at fixed P (i.e. the saddle point equations) give rise to significant changes in the kernels and predictor statistics compared to NNGP regression [37, 14]. Proportional limits in deep Bayesian networks have also been analyzed under the mean field scaling [38, 39].

Transfer Learning in Bayesian Framework Bayesian networks have been studied in a general multi-task framework in NTK parameterization in both lazy and proportional ($P/N = \alpha$) limits [40, 41]. The works [40, 41] first introduced a Bayesian transfer-learning framework in which the target model is regularized to remain in the vicinity of the pre-trained source weights (which are treated as fixed realizations of the source posterior). In these works, when a network is trained on T tasks, the kernels are modulated by a $T \times T$ matrix of scale renormalization constants $Q_{t,t'}(\alpha)$, but individual entries in each task-block of this kernel do not change (compared to the NNGP). In [42] the authors analyze deep linear models on synthetic data, proving that gradient flow under mean-field scaling converges to the Bayes-optimal predictor and showing that positive transfer learning depends on feature similarity between source and target tasks. However, currently no theory has been developed for transfer learning for feature learning non-linear networks obtained from the infinite width limit of mean-field/ μP networks on real datasets.

Continual Learning Dynamics Gradient descent training under continual learning in large width networks under mean-field scaling has been studied in [43]. This analysis revealed that richer training dynamics could lead to more catastrophic forgetting in a sequential multi-task learning, where the task distribution shifts over training time. Average accuracy across tasks was often maximized at an intermediate feature learning strength. However, these results have not yet been studied within a theoretical framework.

2 Theory of Transfer Learning in Infinite Width Two Layer Networks

2.1 Problem Setup

We start by describing our problem setup. We will consider two layer non-linear networks that learn a dataset, respectively $\mathcal{T}_1 = \{\bar{\mathbf{x}}_\mu, \bar{y}_\mu\}_{\mu=1}^{P_1}$ for the pre-trained model and $\mathcal{T}_2 = \{\mathbf{x}_\mu, y_\mu\}_{\mu=1}^{P_2}$ for the downstream task, composed of P_1 and P_2 input-output pairs respectively. We are interested in the regime where $P_1 \geq P_2$. We define the output of our MLP as

$$f_\mu = \frac{1}{\gamma_0 N} \mathbf{w} \cdot \phi \left(\frac{1}{\sqrt{D}} \mathbf{W} \mathbf{x}_\mu \right), \quad (1)$$

where $\mathbf{x}_\mu \in \mathbb{R}^D$ is a D -dimensional input vector, $\mathbf{W} \in \mathbb{R}^{N \times D}$ is the first layer of weights to be learned, $\phi(\cdot)$ is a generic non-linear activation function, and $\mathbf{w} \in \mathbb{R}^N$ is the last layer weight vector. The same network parameterization is applied for the source model, whose collection of weights $\bar{\boldsymbol{\theta}} = \text{Vec}\{\bar{\mathbf{W}}, \bar{\mathbf{w}}\}$. We will indicate variables from the source model with $\bar{\cdot}$ notation.

In both settings we will consider, either the adaptive Neural Bayesian kernel (aNBK [14]) framework (different from the NNGP lazy kernel of [28]) or gradient descent dynamics of randomly initialized networks, both the source and target weights are Gaussian $W_{ij} \sim \mathcal{N}(0, 1)$ under the prior, such that in the infinite width limit $N \rightarrow \infty$ the preactivation entries $\{\bar{h}_i, h_i\}_{i=1}^N$ evolve by $\Theta_N(1)$. This corresponds to the Bayesian version of μP /mean-field scaling for neural networks [44, 10, 26]. We rescale the network output by $\gamma_0 N$ and use a learning rate $\eta = \eta_0 \gamma_0^2 N$ for the discretized dynamics accordingly to the mean-field (μP) parameterization [10, 45, 44, 46]. Here, $\gamma_0 = \Theta_N(1)$ tunes the feature learning strength on a given task $\mathcal{T}_{1/2}$, allowing the preactivations to evolve during training in a task-dependent manner. In principle, we will allow the pre-trained and target models to learn with different richness parameters $\{\bar{\gamma}_0, \gamma_0\}$.

2.2 A Bayesian Framework for Transfer Learning in Two Layer Networks

Result 1 Consider a two layer MLP sampled from the aNBK Bayes posterior [14] for the source task \mathcal{T}_1 , generating sampled weights $\bar{\boldsymbol{\theta}} = \{\bar{\mathbf{W}}, \bar{\mathbf{w}}\}$ from density

$$p(\bar{\boldsymbol{\theta}}) \propto \exp\left(-\frac{\beta N \gamma_0^2}{2} \mathcal{L}(\bar{\boldsymbol{\theta}}, \mathcal{T}_1) - \frac{\lambda}{2} \|\bar{\boldsymbol{\theta}}\|^2\right). \quad (2)$$

Subsequently, sample new weights $\boldsymbol{\theta} = \{\mathbf{W}, \mathbf{w}\}$ from the aNBK Bayes posterior for the target task \mathcal{T}_2 with an elastic penalty $\frac{\delta}{2} \|\mathbf{W} - \bar{\mathbf{W}}\|^2$ between source and target hidden weights in the log-prior

$$p(\boldsymbol{\theta}|\bar{\boldsymbol{\theta}}) \propto \exp\left(-\frac{\beta N \gamma_0^2}{2} \sum_{\mu=1}^{P_2} \mathcal{L}(\boldsymbol{\theta}, \mathcal{T}_2) - \frac{\lambda}{2} \|\boldsymbol{\theta}\|^2 - \frac{\delta}{2} \|\mathbf{W} - \bar{\mathbf{W}}\|^2\right). \quad (3)$$

In the infinite width $N \rightarrow \infty$ limit with square loss, the predictor $f(\mathbf{x}_0)$ on test point \mathbf{x}_0 is a kernel predictor

$$f(\mathbf{x}_0) = \sum_{\mu, \nu \in \mathcal{T}_2} \Phi(\mathbf{x}_0, \mathbf{x}_\mu) (\boldsymbol{\Phi} + \beta^{-1} \mathbf{I})_{\mu\nu}^{-1} y_\nu \quad (4)$$

where $\boldsymbol{\Phi} \in \mathbb{R}^{P_2 \times P_2}$ is the **adapted feature kernel**, which depends on both tasks \mathcal{T}_1 and \mathcal{T}_2 . The feature kernel can be obtained by solving a min-max problem $\min_{\boldsymbol{\Phi}} \max_{\hat{\boldsymbol{\Phi}}} \mathcal{F}[\boldsymbol{\Phi}, \hat{\boldsymbol{\Phi}}]$ where the function \mathcal{F} is

$$\begin{aligned} \mathcal{F}[\boldsymbol{\Phi}, \hat{\boldsymbol{\Phi}}] &= -\frac{1}{2} \text{Tr}(\boldsymbol{\Phi} \hat{\boldsymbol{\Phi}}) + \frac{\gamma_0^2}{2} \mathbf{y}^\top \left(\boldsymbol{\Phi} + \frac{\mathbf{I}}{\beta}\right)^{-1} \mathbf{y} - \mathbb{E}_{\bar{\mathbf{h}}} \ln \mathcal{Z}_2[\bar{\mathbf{h}}], \\ \mathcal{Z}_2[\bar{\mathbf{h}}] &= \int d\mathbf{h} \exp\left(-\frac{1}{2} \left(\mathbf{h} - \frac{\delta}{1+\delta} \bar{\mathbf{h}}\right)^\top \left(\frac{\mathbf{C}^{(2,2)}}{1+\delta}\right)^{-1} \left(\mathbf{h} - \frac{\delta}{1+\delta} \bar{\mathbf{h}}\right) - \frac{1}{2} \phi(\mathbf{h})^\top \hat{\boldsymbol{\Phi}} \phi(\mathbf{h})\right), \\ C_{\mu\nu}^{(2,2)} &\equiv \frac{1}{D} \mathbf{x}_\mu \cdot \mathbf{x}_\nu, \end{aligned} \quad (5)$$

where $C_{\mu\nu}^{(2,2)}$ is the data Gram matrix for all pairs of inputs $\mathbf{x}_\mu, \mathbf{x}_\nu \in \mathcal{T}_2$ and the average $\mathbb{E}_{\bar{\mathbf{h}}}$ represents an average over the hidden preactivation distribution $\bar{\mathbf{h}}$ induced by the source hidden weights on the target task data \mathcal{T}_2 . The distribution of $\bar{\mathbf{h}}$ is itself obtained as a solution to a min-max problem involving only the source task \mathcal{T}_1 following [14].

A detailed derivation of this result is given in Appendix C. To derive this result, we study the limiting free energy $\mathcal{F}[\bar{\mathbf{W}}]$ for the target task, which depends explicitly on the source task weights $\bar{\mathbf{W}}$,

$$\mathcal{F}[\bar{\mathbf{W}}] = - \lim_{N \rightarrow \infty} \frac{1}{N} \ln Z[\bar{\mathbf{W}}]. \quad (6)$$

The partition function $Z[\bar{\mathbf{W}}]$ defines the aNBK Bayes posterior over the target-task parameters $\boldsymbol{\theta} = \{\mathbf{W}, \mathbf{w}\}$ at a given source weight $\bar{\mathbf{W}}$

$$Z[\bar{\mathbf{W}}] = \int d\boldsymbol{\theta} \exp\left(-\frac{\beta N \gamma_0^2}{2} \sum_{\mu=1}^{P_2} \mathcal{L}(\boldsymbol{\theta}, \mathcal{T}_2) - \frac{\lambda}{2} \|\boldsymbol{\theta}\|^2 - \frac{\delta}{2} \|\mathbf{W} - \bar{\mathbf{W}}\|^2\right). \quad (7)$$

In principle, $\mathcal{F}[\bar{\mathbf{W}}]$ is a random variable, but fortunately in the $N \rightarrow \infty$ limit, the free energy concentrates around its average $\mathcal{F} = \mathbb{E}_{\bar{\mathbf{W}} \sim p(\bar{\boldsymbol{\theta}}|\mathcal{T}_1)} \mathcal{F}[\bar{\mathbf{W}}]$ which can be computed using the replica trick [47, 48]. This average will capture the typical behavior of draws of $\bar{\mathbf{W}}$ from the posterior distribution of weights for the source task \mathcal{T}_1 under a Gaussian prior $\bar{W}_{ij}, \bar{w}_j \sim \mathcal{N}(0, 1)$, which itself can be characterized using statistical mechanics [14] (see Appendix C). Consistent with prior Bayesian network theory [13, 37, 14], Eq. (6) is function of two matrix order parameters $\boldsymbol{\Phi}, \hat{\boldsymbol{\Phi}} \in \mathbb{R}^{P_2 \times P_2}$. The matrix $[\boldsymbol{\Phi}]_{\mu\nu} = \frac{1}{N} \sum_{i=1}^N \phi(h_{i,\mu}) \phi(h_{i,\nu})$ is the **adapted feature kernel** for the hidden layer and $\hat{\boldsymbol{\Phi}}$ is its conjugate variable [14]. In the infinite width limit $N \rightarrow \infty$ the free energy is dominated by a set of saddle point equations, which are the solution to a min-max optimization problem over $\min_{\boldsymbol{\Phi}} \max_{\hat{\boldsymbol{\Phi}}} \mathcal{F}[\boldsymbol{\Phi}, \hat{\boldsymbol{\Phi}}]$. The saddle point equations, which describe the $N \rightarrow \infty$ limit, are

$$\begin{aligned} \frac{\partial}{\partial \hat{\boldsymbol{\Phi}}} \mathcal{F}[\boldsymbol{\Phi}, \hat{\boldsymbol{\Phi}}] &= \hat{\boldsymbol{\Phi}} - \mathbb{E}_{\bar{\mathbf{h}}} \left[\mathbb{E}_{\mathbf{h}|\bar{\mathbf{h}}} \phi(\mathbf{h}) \phi(\mathbf{h})^\top \right] = 0, \\ \frac{\partial}{\partial \boldsymbol{\Phi}} \mathcal{F}[\boldsymbol{\Phi}, \hat{\boldsymbol{\Phi}}] &= \hat{\boldsymbol{\Phi}} + \gamma_0^2 \left(\frac{\mathbf{I}}{\beta} + \boldsymbol{\Phi}\right)^{-1} \mathbf{y} \mathbf{y}^\top \left(\frac{\mathbf{I}}{\beta} + \boldsymbol{\Phi}\right)^{-1} = 0, \end{aligned} \quad (8)$$

where $\mathbf{h}|\bar{\mathbf{h}}$ is the distribution defined by the single-site moment generating function \mathcal{Z}_2 in Result 1 while $\mathbb{E}_{\bar{\mathbf{h}}}$ refers to the average over the source field distribution on the target task \mathcal{T}_2 (see Appendix C for details). In general, this single site density is non-Gaussian. As a result, the adaptive kernel Φ collects all higher moments of the activation distribution, which are shifted by both the source fields $\bar{\mathbf{h}}$ and the term involving the dual kernel $\hat{\Phi}$. However, in the lazy limit $\gamma_0 \rightarrow 0$, the dual kernel vanishes $\hat{\Phi} \rightarrow 0$ and the preactivation distribution $p(\mathbf{h}|\bar{\mathbf{h}})$ simply recovers a Gaussian distribution $p(\mathbf{h}|\bar{\mathbf{h}}) \sim \mathcal{N}(\frac{\delta}{1+\delta}\bar{\mathbf{h}}, \frac{\mathbf{C}^{(2,2)}}{1+\delta})$ with shifted mean and rescaled covariance, both dependent on the transfer from \mathcal{T}_1 . Moreover, when both $\gamma_0 = \delta = 0$ we recover an unstructured Gaussian process $p(\mathbf{h}|\bar{\mathbf{h}}) \sim \mathcal{N}(0, \mathbf{C}^{(2,2)})$ [28]. As clarified in Appendix C.4, knowing the form of the free energy in Eq. (6) makes it easy to compute the *deterministic predictor* of the target model on a new unseen sample $\{\mathbf{x}_0, y_0\}$, which turns out to be a kernel regression predictor with the adapted target task kernel $\Phi(x, x')$ as in Eq. (4). Consistently with [14], $\Phi(\mathbf{x}_0) = \mathbb{E}_{\bar{\mathbf{h}_0, \bar{\mathbf{h}}}} \left[\mathbb{E}_{h_0, \mathbf{h}|\bar{\mathbf{h}_0, \bar{\mathbf{h}}}} \phi(h_0)\phi(\mathbf{h}) \right]$ is the kernel between the test point \mathbf{x}_0 and the training data $\{\mathbf{x}_\mu\}_{\mu=1}^{P_2} \in \mathcal{T}_2$ (see Appendix C.4).

2.3 Two Stage Gradient Flow Dynamics for Transfer Learning

Result 2 Consider a two-layer MLP with parameters $\bar{\theta} = \text{Vec}(\bar{\mathbf{W}}, \bar{\mathbf{w}})$, trained on a source task \mathcal{T}_1 from random initial conditions $\bar{W}_{ij}(0), \bar{w}_j(0) \sim \mathcal{N}(0, 1)$ under gradient flow with weight decay $\frac{d\bar{\theta}}{dt} = -\bar{\gamma}_0^2 N \nabla_{\bar{\theta}} \mathcal{L} - \lambda \bar{\theta}$ and up to a time \bar{t} . Subsequently, a target model with parameters θ is trained on a downstream task \mathcal{T}_2 from random initial conditions for the readout weights $w_i \sim \mathcal{N}(0, 1)$ and source initial conditions for hidden weights $\mathbf{W}(0) = \bar{\mathbf{W}}$. The infinite width $N \rightarrow \infty$ dynamics of this second model under gradient flow, with weight decay and an elastic penalty $\frac{\delta}{2} |\mathbf{W}(t) - \bar{\mathbf{W}}|^2$ only on the first layer weights, converges after a training time t to a predictor $f(\mathbf{x}_0, t)$ on a test point \mathbf{x}_0

$$f(\mathbf{x}_0, t) = \gamma_0^{-1} \mathbb{E}_{\psi, \{\bar{h}_\mu\}_{\mu \in \mathcal{P}_2}} [z(t)\phi(h_0(t))] \quad (9)$$

where the preactivations and the readout variables evolve as stochastic processes

$$\begin{aligned} h_\mu(t) &= e^{-(\lambda+\delta)t} \bar{h}_\mu + \frac{\delta}{\lambda+\delta} \left(1 - e^{-(\lambda+\delta)t}\right) \bar{h}_\mu + \gamma_0 \int_0^t ds e^{-(\lambda+\delta)(t-s)} \sum_{\nu \in \mathcal{T}_2} \Delta_\nu(s) g_\nu(s) C_{\mu\nu}^{(2,2)}, \\ z(t) &= e^{-\lambda t} \psi + \gamma_0 \int_0^t e^{-\lambda(t-s)} \sum_{\mu \in \mathcal{T}_2} \Delta_\mu(s) \phi(h_\mu(s)), \\ g_\mu(t) &= \dot{\phi}(h_\mu(t)) z(t) \end{aligned} \quad (10)$$

being $C_{\mu\nu}^{(2,2)}$ the data Gram matrix as in Eq. (5). The average $\mathbb{E}_{\psi, \{\bar{h}_\mu\}_{\mu \in \mathcal{P}_2}}$ is over both $\psi = w_i(0) \sim \mathcal{N}(0, 1)$ and $\{\bar{h}_\mu\}$, defined with its own stochastic process by evolving the DMFT equations on the source task \mathcal{T}_1 up to a time \bar{t} as in [26]. $\Delta_\mu(t) = y_\mu - f_\mu(t)$ represents the error signal for a pattern $\mu \in \mathcal{T}_2$, and g_μ are the entries of the gradient vector $\mathbf{g}_\mu(t) = N \gamma_0 \frac{\partial f}{\partial \mathbf{h}_\mu}$.

A detailed derivation of this result is given in Appendix D and as an extension of [26]. To get this result, the first layer weight dynamics we consider on \mathcal{T}_2 takes the form

$$\frac{d\mathbf{W}(t)}{dt} = -\frac{\gamma^2}{N} \sum_{\mu \in \mathcal{T}_2} \Delta_\mu(t) \mathbf{g}_\mu(t) \mathbf{x}_\mu^\top - \lambda \mathbf{W}(t) - \delta (\mathbf{W}(t) - \bar{\mathbf{W}}). \quad (11)$$

The above weight dynamics induces dynamics for the $h_\mu(t)$ variables. In the infinite width limit $N \rightarrow \infty$, the N neurons become statistically independent and the predictions $f(x, t)$ concentrate. The predictor value can be determined by keeping track of the preactivations and readout variables (see Appendix D).

3 Transfer Learning Phenomenology

In the following, we illustrate the interplay between transfer learning, feature learning strength, sample size and task similarity leveraging our theoretical results in Section 2. We start with controlled settings where the data is generated by teacher-student setups of increasing complexity, and then conclude with real datasets.

3.1 Transfer Learning of Linear Tasks with Linear Activations

Linear neural networks (where $\phi(h) \equiv h$) are the simplest analytically tractable models of feature learning [49, 50, 22, 37, 29, 51, 52]. In our setting, given linear activations, the distribution of preactivations remains Gaussian at each layer when $P = \Theta_N(1)$ due to the Central Limit Theorem. Because of this property, in the Bayesian framework the saddle point equations for the kernels of the downstream task (\mathcal{T}_2) simplify (see Appendix C.5):

$$\begin{aligned} \hat{\Phi} &= \left[(1 + \delta) \mathbf{C}^{-1} + \hat{\Phi} \right]^{-1} + \delta^2 \left[(1 + \delta) \mathbf{C}^{-1} + \hat{\Phi} \right]^{-1} \mathbf{C}^{-1} \mathbb{E}_{\bar{\mathbf{h}} \sim p(\bar{\mathbf{h}})} (\bar{\mathbf{h}}_2 \bar{\mathbf{h}}_2^\top) \mathbf{C}^{-1} \left[(1 + \delta) \mathbf{C}^{-1} + \hat{\Phi} \right]^{-1} \\ \hat{\Phi} &= -\gamma_0^2 \left(\frac{\mathbf{I}}{\beta} + \hat{\Phi} \right)^{-1} \mathbf{y} \mathbf{y}^\top \left(\frac{\mathbf{I}}{\beta} + \hat{\Phi} \right)^{-1}, \end{aligned} \quad (12)$$

where in the above equation $\mathbf{C} = \mathbf{C}^{(2,2)}$ is the target task Gram matrix (Eq. (5)) and \mathbf{y} is the target-task labels. The dependence on the source task enters through $\bar{\mathbf{h}}_2 \in \mathbb{R}^{P_2}$, which are the preactivations for the source model on target task \mathcal{T}_2 data. The expectation is taken over $p(\bar{\mathbf{h}}) \sim \mathcal{N}(0, (\mathbf{C}_{\mathcal{T}_1 \cup \mathcal{T}_2}^{-1} + \hat{\Phi}_{\mathcal{T}_1})^{-1})$.

It is instructive to consider the lazy limit where $\gamma_0 \rightarrow 0$. Here, the dual kernel $\hat{\Phi}$ vanishes and Eq. (12) reduces to $\hat{\Phi} = \frac{1}{(1+\delta)} \mathbf{C} + \frac{\delta^2}{(1+\delta)^2} \mathbb{E}_{\bar{\mathbf{h}}} (\bar{\mathbf{h}}_{\mathcal{T}_2} \bar{\mathbf{h}}_{\mathcal{T}_2}^\top)$. When $\delta \rightarrow \infty$, the network is solving a kernel regression on \mathcal{T}_2 with the fixed (adaptive) feature kernel produced by the pre-training on \mathcal{T}_1 . When $\delta \rightarrow 0$, the network is solving a kernel regression on \mathcal{T}_2 with the fixed feature kernel induced by random linear features. For intermediate values of δ , the network still solves a kernel regression problem with a kernel interpolating between these two limiting kernels. By contrast, in the feature-learning regime ($\gamma_0 = \Theta_N(1)$) the downstream task feature adaptation and the elastic coupling δ interact in a non-trivial way, producing kernels that integrate representations on both \mathcal{T}_1 and \mathcal{T}_2 .

A clear example of this is the simplest possible case where $\mathcal{T}_1 \equiv \mathcal{T}_2$, the input data are whitened $\mathbf{C}^{(1,1)} = \mathbf{C}^{(2,2)} = \mathbf{I} \in \mathbb{R}^{P \times P}$ and the labels are normalized $|\mathbf{y}|^2 = 1$. We show in Appendix C.5, that in this setting the equations get simplified even further since both source $\{\hat{\Phi}, \hat{\Phi}\}$ and target $\{\hat{\Phi}, \hat{\Phi}\}$ kernels only grow in the rank-one direction $\mathbf{y} \mathbf{y}^\top$. As a consequence, one can only keep track of the overlaps with the label direction $\mathbf{y}^\top \hat{\Phi} \mathbf{y} = \phi$ and $\mathbf{y}^\top \hat{\Phi} \mathbf{y} = \hat{\phi}$. For the target \mathcal{T}_2 we get

$$\phi = (1 + \delta + \hat{\phi})^{-1} + \delta^2 \bar{\phi} (1 + \delta + \hat{\phi})^{-2}, \quad \hat{\phi} = -\gamma_0^2 (\beta^{-1} + \phi)^{-2}. \quad (13)$$

The saddle point equations for the kernels of \mathcal{T}_1 were derived in [14] and can be found in Appendix C. When $\delta \rightarrow \infty$ the target model strongly relies on the features learned from \mathcal{T}_1 and $\phi = \bar{\phi}$ as expected. We simulate this model in Figure 1, where we allow the pre-trained model to learn with a feature strength γ_s different from γ_t of the target model. When the source is richer than the target ($\gamma_s > \gamma_t$), increasing the elastic coupling monotonically increase the label alignment ϕ . If instead the target is richer ($\gamma_s < \gamma_t$), the contrary happens and the optimum occurs at $\delta = 0$. In the balanced case $\gamma_s = \gamma_t$, ϕ remains almost flat, rising only marginally with δ under our low-data regime.

Task similarity. By slightly increasing the task complexity for the same linear models, we generate a dataset $\{\mathbf{x}_\mu, \mathbf{y}_\mu\}_{\mu=1}^{P_2}$ from a population distribution $\mathbf{x}_\mu \sim \mathcal{N}(0, \mathbf{I}_D)$ by setting $\mathbf{y}_\mu = \mathbf{w} \cdot \mathbf{x}_\mu$ with $\|\mathbf{w}\|_2 = 1$. Here, the task vector \mathbf{w} is partially aligned with the source task vector β (s.t. $\|\beta\|_2 = 1$) who generated the source labels of \mathcal{T}_1 according to $\bar{\mathbf{y}}_\mu = \beta \cdot \mathbf{x}_\mu$, such that $\beta \cdot \mathbf{w} = \alpha$. In Fig. 2 we show that, for $P_1 > P_2$ and $\gamma_s = \gamma_t$, the effect of transfer learning is to improve the test loss performance for $\alpha > 0$. When $\alpha = 0$ and the source and target task vectors are orthogonal, transfer learning has no effect on the test loss, because in order to interpolate on \mathcal{T}_2 , the model needs to learn a new direction \mathbf{w} without any prior knowledge. In the extreme case where $P_1 = P_2$ and $\bar{\mathbf{y}} \cdot \mathbf{y} = m$ the kernels can be studied by tracking their overlaps with the span $\{\bar{\mathbf{y}}, \mathbf{y}\}$ directions (see Appendix C.5).

3.2 Transfer Learning of Polynomial Tasks with Nonlinear Activations

Low to High Degree Polynomials Kernel limits of neural networks are strongly biased to fit their data with low degree polynomials when data is high dimensional and isotropic. This spectral bias [53, 15, 20] reflects the fact that kernel methods learn eigenfunctions in order of decreasing eigenvalue [54, 55, 56]. By contrast, networks trained in the feature-learning regime can learn sparse

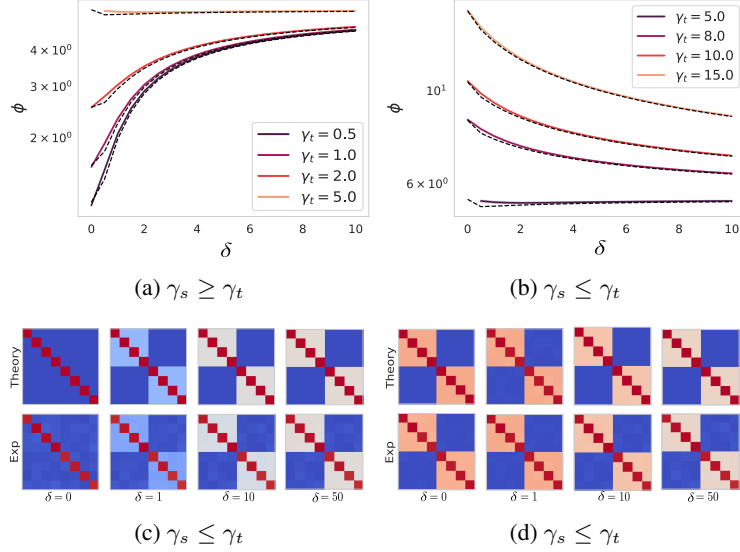


Figure 1: Transfer learning for linear networks trained on whitened data $\mathbf{C} = \mathbf{I}$ increases the overlap ϕ with the label direction $\mathbf{y}^\top \Phi \mathbf{y} = \phi$ if the source is richer than the target model. (a)/(b) Overlaps ϕ vs elastic constraint δ for a two-layer linear model trained on $P = 8$ patterns with $\mathbf{y} = \{\pm 1\}^P$. Source network is pre-trained on the same data as the target, with a richness parameter $\gamma_s = 5.0$. Solid lines taken from Langevin dynamics on $N = 20000$ network, dashed lines from the Bayesian theory. (c)/(d) Examples of learned kernels as a function of the elastic coupling δ .

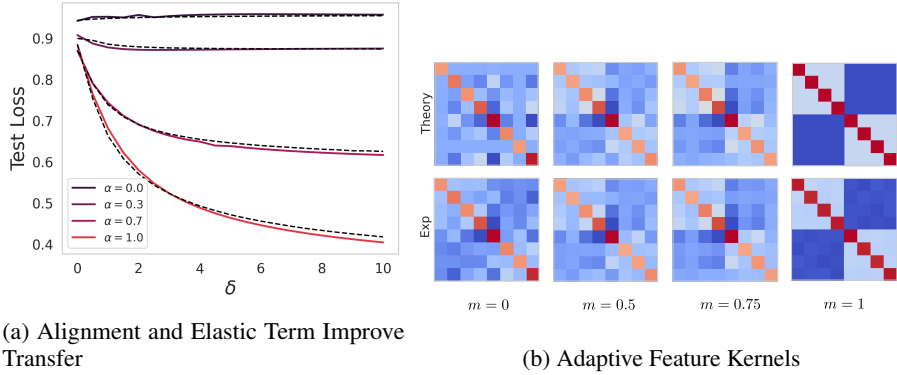


Figure 2: The benefit of transfer learning increases with the similarity between source and target tasks. (a) Test losses of a two-layer linear model as a function of the elastic coupling δ for different levels α of task-similarity. Data are generated from an isotropic Gaussian distribution $\mathbf{x} \sim \mathcal{N}(0, \mathbf{I})$. Target vector is given by a linear model $\mathbf{y} = \mathbf{w} \cdot \mathbf{x}$ with $\|\mathbf{w}\|_2 = 1$. Here, the target depends on the source task vector β (such that $\|\beta\|_2 = 1$) by the relation $\mathbf{w} = \alpha\beta + \sqrt{1 - \alpha^2}\mathbf{w}_\perp$ where $\mathbf{w} \cdot \mathbf{w}_\perp = 0$. Solid lines taken from Langevin dynamics on $N = 20000$ network, black dashed lines from Bayesian theory. (b) Target kernels as a function of task similarity $m = \bar{\mathbf{y}} \cdot \mathbf{y}$.

polynomials from much fewer data and training steps [44, 57, 58, 59]. The staircase property [60, 61, 62, 63] explored by [57] makes this hierarchy explicit in multi-index polynomial settings.

Inspired by the utility of feature learning on sparse polynomials of Gaussian data $\mathbf{x} \sim \mathcal{N}(0, \mathbf{I})$, we explore transfer learning in this setting where learned features from the source task could promote performance on the target task. In Fig. 3 we show that first learning a linear function $y_1(\mathbf{x}) = \frac{1}{\sqrt{D}}\beta \cdot \mathbf{x}$ before learning a quadratic teacher function $y_2(\mathbf{x}) = \left(\frac{1}{\sqrt{D}}\beta \cdot \mathbf{x}\right)^2$ can improve performance when $\delta > 0$ and P_2 is small (Fig. 3). The same happens with Hermite polynomial teachers $y_2(\mathbf{x}) = \text{He}_k\left(\frac{1}{\sqrt{D}}\beta \cdot \mathbf{x}\right)$ of increasing degree k . Fig. 4 shows that learning and $\delta > 0$

when the pre-trained task is of lower complexity than the target, allows the model to generalize better compared to the performance of a model randomly initialized ($\delta = 0$).

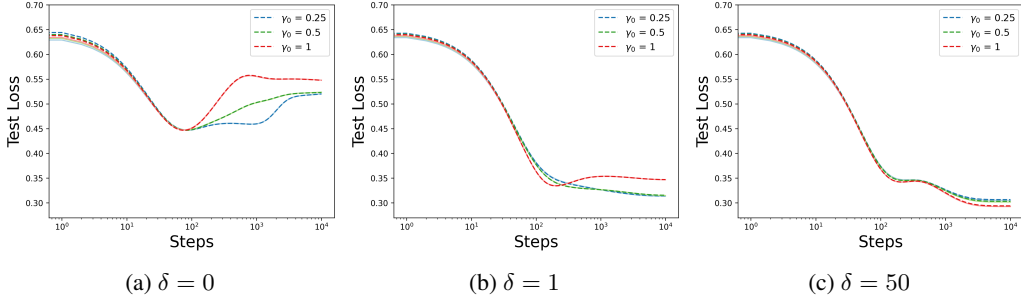


Figure 3: Low degree polynomial teacher model on source task $y_1(\mathbf{x}) = \frac{1}{\sqrt{D}}\boldsymbol{\beta} \cdot \mathbf{x}$ with $P_1 = 1000$ and $D = 75$. Target task is $y_2(\mathbf{x}) = (\frac{1}{\sqrt{D}}\boldsymbol{\beta} \cdot \mathbf{x})^2$ with $P_2 = 20$. Test losses of a two-layer ReLU MLP vs number of training steps. (a): Random initialization, i.e. $W_{ij} \sim \mathcal{N}(0, 1)$ and no elastic penalty $\delta = 0$. (b)-(c): Dynamics starting from $\mathbf{W} = \bar{\mathbf{W}}$ for $\delta = 1$ and $\delta = 50$. Solid lines taken from gradient descent dynamics on $N = 20000$ network, dashed lines from DMFT theory.

High to Low Degree Polynomials Despite the benefit of transfer learning when going from low degree to high degree polynomials, transfer learning can be disadvantageous when going from high degree to low degree. In Fig. 5, we compare the model performances when learning a low degree Hermite polynomial target function from either a random initial condition and $\delta = 0$, or the features learned from a high degree Hermite source task. In the first case, learning the target from a random start is speeded up by feature learning strength γ_0 on \mathcal{T}_1 . Similarly to a grokking phenomena[64, 65, 66, 67], we conjecture that in this initial training phase the network begins memorizing its training set and slightly overfit, then after adapts features to the data, leading to improved test loss at late times. This adaptations of features happens faster when training with higher γ_0 . On the contrary, when $\delta > 0$, initializing from the high-degree features forces the network to rely on spurious high-frequency components that are not needed by the simpler task. The elastic coupling prevents the model from discarding these overly complex features, so test-loss curves either plateau at higher values when feature learning strength is small (small γ_0) or decrease more slowly than in the random-init and $\delta = 0$ case. However, as visible in Fig. 5, a sufficiently large feature-learning strength (the red curve, high γ_0) can overcome this “bad” initialization: strong feature adaptation gradually realigns the pre-trained weights with the lower-degree target manifold, eventually recovering and even matching, the generalization performance of the $\delta = 0$ model.

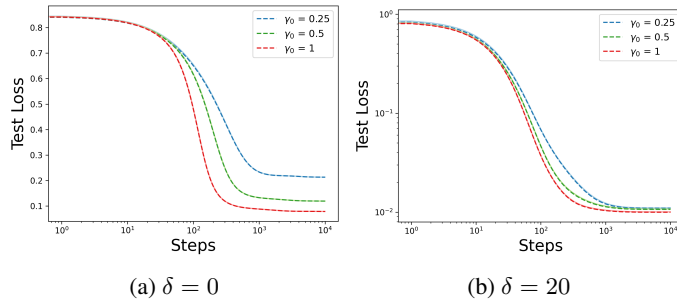


Figure 4: Comparison of (a) training from random initialization versus (b) training from a warm-start and $\delta > 0$ on Hermite regression tasks, from easy to hard. Source task: $y_1(\mathbf{x}) = \text{He}_2\left(\frac{1}{\sqrt{D}}\boldsymbol{\beta}_1 \cdot \mathbf{x}\right)$ with $P_1 = 1000$ and $\bar{\gamma}_0 = 1.0$. Target task: $y_2(\mathbf{x}) = \text{He}_3\left(\frac{1}{\sqrt{D}}\boldsymbol{\beta}_2 \cdot \mathbf{x}\right)$ with $P_2 = 200$ and multiple feature learning strengths γ_0 . Solid lines taken from gradient descent dynamics on $N = 20000$ two-layer ReLU network, dashed lines from DMFT theory.

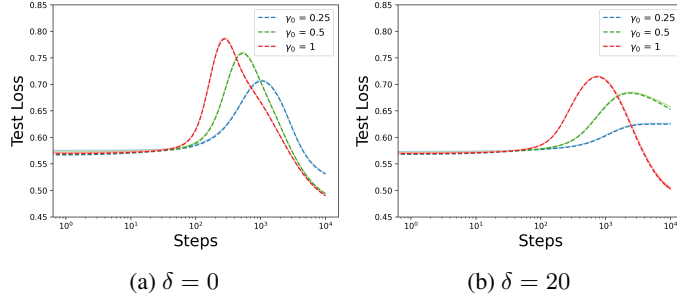


Figure 5: Comparison of (a) training from random initialization versus (b) training from a warm-start and $\delta > 0$ on Hermite regression tasks, from hard to easy. Source task: $\text{He}_5(\beta_1 \cdot \mathbf{x})$ with $P_1 = 1000$ and $\bar{\gamma}_0 = 1.0$. Target task: $\text{He}_2(\beta_2 \cdot \mathbf{x})$ with $P_2 = 400$ and $\beta_1 \cdot \beta_2 = 0.8$. Solid lines: gradient-descent on an $N = 20000$ two-layer ReLU network. Dashed lines: DMFT theory.

3.3 Role of Transfer Learning on real datasets

Moving beyond synthetic tasks, we consider simple image classification problems. We start with CIFAR-10, where a model pretrained on two source classes is fine-tuned on two disjoint target classes. In Fig. 6, for every feature-learning strength γ_0 the downstream test loss falls monotonically as δ increases, indicating improvements due to transfer learning. The best performance is achieved at large δ and large γ_0 , showing that the combination of strong elastic penalties and rich training yields the lowest loss. In Fig. 6 the distribution of the preactivations $p(h)$ on the target shows that, as δ grows, $p(h)$ broadens and develops heavier tails. Intuitively, mixing in the pretrained filters injects higher-variance components into the representation, so that activations span a wider range even as the network learns task-specific structure.

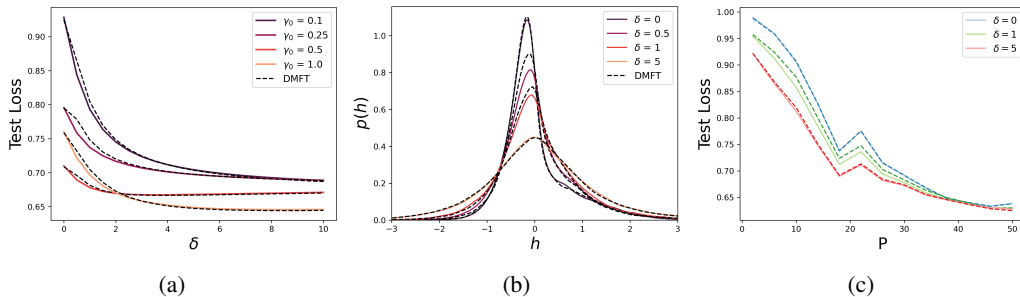


Figure 6: (a) Transfer learning is beneficial for real tasks at any feature learning strength γ_0 . Source task: classes 1/2 of CIFAR-10 with $P_1 = 1000$ and $\bar{\gamma}_0 = 1.0$. Target task: classes 8/9 of CIFAR-10 with $P_2 = 50$. (b) Preactivation distribution of the target model for different δ . Solid lines: GD at convergence ($N = 20000$, 2-layer NN); black dashed lines: DMFT. (c) Transfer and feature learning ($\gamma_0 = 0.5$) as a function of target-task sample size P_2 .

Fig. 6(c) examines how benefits from transfer learning vary with the number of downstream samples P_2 . When feature learning is weak ($\gamma_0 = 0.5$, left panel), $\delta > 0$ delivers a large gain at small P_2 , and the model relies on the source priors to offset the effect of data scarcity.

4 Discussion and Conclusion

In this work we developed a theory of transfer learning in infinite width neural networks. The theory utilizes an elastic weight penalty for the hidden weight matrices between the source and target tasks. We find that transfer learning is often best when both the elastic weight penalty and the richness of optimization in the target task are high. Our results illustrate how task similarity controls the relative benefits of transfer learning compared to learning from scratch. For linear and polynomial tasks, the task similarity is governed by the alignment of the label generating function for source and target tasks, while for image data we manipulate task similarity by changing the classes which are included in the classification problem.

Connections to Fine tuning Fine tuning a model for a downstream task is a common practice in computer vision and language processing. In our theory if target-task training is lazy $\gamma_0 \rightarrow 0$ and the elastic penalty is large $\delta \rightarrow \infty$, then this corresponds to fine tuning with a linear probe [68]. For small δ , the model essentially must learn features from scratch during the transfer task. While our current theory describes fine tuning every parameter in the model with gradient descent, future work could explore a theory for low-rank fine tuning methods, which are becoming increasingly popular for large pretrained models [69].

Limitations This present work is limited for many reasons. First, our focus in this paper is on two layer networks. Future work could explore how representation learning in deeper networks enable transfer learning. Specifically, it could be interesting to study what number of hidden layers should be preserved during transfer learning [70]. Second, our theory currently does not average over the dataset so the theoretical equations scale with the number of datapoints. Future work could attempt to average over data for simple target functions such as the linear or polynomial tasks [20].

Acknowledgements and Disclosure of Funding

We would like to thank the members of the Pehlevan lab for useful insights. C.L. is supported by DARPA Award DIAL-FP-038, and The William F. Milton Fund from Harvard University. B.B. is supported by a Google PhD Fellowship and NSF CAREER Award IIS-2239780. C.P. is supported by NSF grant DMS-2134157, NSF CAREER Award IIS-2239780, DARPA Award DIAL-FP-038, a Sloan Research Fellowship, and The William F. Milton Fund from Harvard University. This work has been made possible in part by a gift from the Chan Zuckerberg Initiative Foundation to establish the Kempner Institute for the Study of Natural and Artificial Intelligence.

References

- [1] Joel Hestness, Sharan Narang, Newsha Ardalani, Gregory Diamos, Heewoo Jun, Hassan Kianinejad, Md Mostofa Ali Patwary, Yang Yang, and Yanqi Zhou. Deep learning scaling is predictable, empirically. *arXiv preprint arXiv:1712.00409*, 2017.
- [2] Jared Kaplan, Sam McCandlish, Tom Henighan, Tom B Brown, Benjamin Chess, Rewon Child, Scott Gray, Alec Radford, Jeffrey Wu, and Dario Amodei. Scaling laws for neural language models. *arXiv preprint arXiv:2001.08361*, 2020.
- [3] Jordan Hoffmann, Sebastian Borgeaud, Arthur Mensch, Elena Buchatskaya, Trevor Cai, Eliza Rutherford, Diego de Las Casas, Lisa Anne Hendricks, Johannes Welbl, Aidan Clark, et al. Training compute-optimal large language models. *arXiv preprint arXiv:2203.15556*, 2022.
- [4] Chuanqi Tan, Fuchun Sun, Tao Kong, Wenchang Zhang, Chao Yang, and Chunfang Liu. A survey on deep transfer learning. In *Artificial Neural Networks and Machine Learning—ICANN 2018: 27th International Conference on Artificial Neural Networks, Rhodes, Greece, October 4-7, 2018, Proceedings, Part III* 27, pages 270–279. Springer, 2018.
- [5] Tom Brown, Benjamin Mann, Nick Ryder, Melanie Subbiah, Jared D Kaplan, Prafulla Dhariwal, Arvind Neelakantan, Pranav Shyam, Girish Sastry, Amanda Askell, et al. Language models are few-shot learners. *Advances in neural information processing systems*, 33:1877–1901, 2020.
- [6] Xuhong Li, Yves Grandvalet, Franck Davoine, Jingchun Cheng, Yin Cui, Hang Zhang, Serge Belongie, Yi-Hsuan Tsai, and Ming-Hsuan Yang. Transfer learning in computer vision tasks: Remember where you come from. *Image and Vision Computing*, 93:103853, 2020.
- [7] Berivan Isik, Natalia Ponomareva, Hussein Hazimeh, Dimitris Paparas, Sergei Vassilvitskii, and Sanmi Koyejo. Scaling laws for downstream task performance in machine translation. In *The Thirteenth International Conference on Learning Representations*, 2025.
- [8] Mei Song, Andrea Montanari, and P Nguyen. A mean field view of the landscape of two-layers neural networks. *Proceedings of the National Academy of Sciences*, 115(33):E7665–E7671, 2018.

- [9] Lenaic Chizat and Francis Bach. On the global convergence of gradient descent for over-parameterized models using optimal transport. *Advances in neural information processing systems*, 31, 2018.
- [10] Greg Yang and Edward J Hu. Tensor programs iv: Feature learning in infinite-width neural networks. In *International Conference on Machine Learning*, pages 11727–11737. PMLR, 2021.
- [11] Blake Bordelon and Cengiz Pehlevan. Self-consistent dynamical field theory of kernel evolution in wide neural networks. *Journal of Statistical Mechanics: Theory and Experiment*, 2023(11):114009, 2023.
- [12] Adam X Yang, Maxime Robeyns, Edward Milsom, Ben Anson, Nandi Schoots, and Laurence Aitchison. A theory of representation learning gives a deep generalisation of kernel methods. In *International Conference on Machine Learning*, pages 39380–39415. PMLR, 2023.
- [13] Kirsten Fischer, Javed Lindner, David Dahmen, Zohar Ringel, Michael Krämer, and Moritz Helias. Critical feature learning in deep neural networks. *arXiv preprint arXiv:2405.10761*, 2024.
- [14] Clarissa Lauditi, Blake Bordelon, and Cengiz Pehlevan. Adaptive kernel predictors from feature-learning infinite limits of neural networks. *arXiv preprint arXiv:2502.07998*, 2025.
- [15] Blake Bordelon, Abdulkadir Canatar, and Cengiz Pehlevan. Spectrum dependent learning curves in kernel regression and wide neural networks. In *International Conference on Machine Learning*, pages 1024–1034. PMLR, 2020.
- [16] Abdulkadir Canatar, Blake Bordelon, and Cengiz Pehlevan. Out-of-distribution generalization in kernel regression. *Advances in Neural Information Processing Systems*, 34:12600–12612, 2021.
- [17] Ben Sorscher, Surya Ganguli, and Haim Sompolinsky. Neural representational geometry underlies few-shot concept learning. *Proceedings of the National Academy of Sciences*, 119(43):e2200800119, 2022.
- [18] Oussama Dhifallah and Yue M Lu. Phase transitions in transfer learning for high-dimensional perceptrons. *Entropy*, 23(4):400, 2021.
- [19] Federica Gerace, Luca Saglietti, Stefano Sarao Mannelli, Andrew Saxe, and Lenka Zdeborová. Probing transfer learning with a model of synthetic correlated datasets. *Machine Learning: Science and Technology*, 3(1):015030, 2022.
- [20] Abdulkadir Canatar, Blake Bordelon, and Cengiz Pehlevan. Spectral bias and task-model alignment explain generalization in kernel regression and infinitely wide neural networks. *Nature communications*, 12(1):2914, 2021.
- [21] Arthur Jacot, Franck Gabriel, and Clément Hongler. Neural tangent kernel: Convergence and generalization in neural networks, 2020.
- [22] Sanjeev Arora, Nadav Cohen, Noah Golowich, and Wei Hu. A convergence analysis of gradient descent for deep linear neural networks, 2019.
- [23] Jaehoon Lee, Lechao Xiao, Samuel S Schoenholz, Yasaman Bahri, Roman Novak, Jascha Sohl-Dickstein, and Jeffrey Pennington. Wide neural networks of any depth evolve as linear models under gradient descent *. *Journal of Statistical Mechanics: Theory and Experiment*, 2020(12):124002, December 2020.
- [24] Daniel A Roberts, Sho Yaida, and Boris Hanin. *The principles of deep learning theory*, volume 46. Cambridge University Press Cambridge, MA, USA, 2022.
- [25] Blake Bordelon, Hamza Tahir Chaudhry, and Cengiz Pehlevan. Infinite limits of multi-head transformer dynamics, 2024.
- [26] Blake Bordelon and Cengiz Pehlevan. Self-consistent dynamical field theory of kernel evolution in wide neural networks, 2022.

- [27] Max Welling and Yee Whye Teh. Bayesian learning via stochastic gradient langevin dynamics. In *Proceedings of the 28th International Conference on International Conference on Machine Learning*, ICML'11, page 681–688, Madison, WI, USA, 2011. Omnipress.
- [28] Jaehoon Lee, Yasaman Bahri, Roman Novak, Samuel S. Schoenholz, Jeffrey Pennington, and Jascha Sohl-Dickstein. Deep neural networks as gaussian processes, 2018.
- [29] Qianyi Li and Haim Sompolinsky. Statistical mechanics of deep linear neural networks: The backpropagating kernel renormalization. *Physical Review X*, 11(3), September 2021.
- [30] R. Pacelli, S. Ariosto, M. Pastore, F. Ginelli, M. Gherardi, and P. Rotondo. A statistical mechanics framework for bayesian deep neural networks beyond the infinite-width limit. *Nature Machine Intelligence*, 5(12):1497–1507, December 2023.
- [31] P. Baglioni, R. Pacelli, R. Aiudi, F. Di Renzo, A. Vezzani, R. Burioni, and P. Rotondo. Predictive power of a bayesian effective action for fully connected one hidden layer neural networks in the proportional limit. *Phys. Rev. Lett.*, 133:027301, Jul 2024.
- [32] Qianyi Li and Haim Sompolinsky. Globally gated deep linear networks. *Advances in Neural Information Processing Systems*, 35:34789–34801, 2022.
- [33] Riccardo Aiudi, Rosalba Pacelli, Alessandro Vezzani, Raffaella Burioni, and Pietro Rotondo. Local kernel renormalization as a mechanism for feature learning in overparametrized convolutional neural networks. *Nature Communications*, 16, 2023.
- [34] Noa Rubin, Inbar Seroussi, and Zohar Ringel. Grokking as a first order phase transition in two layer networks. In *The Twelfth International Conference on Learning Representations*, 2024.
- [35] Inbar Seroussi, Gadi Naveh, and Zohar Ringel. Separation of scales and a thermodynamic description of feature learning in some cnns. *Nature Communications*, 14(1):908, 2023.
- [36] Luisa Andreis, Federico Bassetti, and Christian Hirsch. Ldp for the covariance process in fully connected neural networks, 2025.
- [37] Laurence Aitchison. Why bigger is not always better: on finite and infinite neural networks, 2020.
- [38] Noa Rubin, Zohar Ringel, Inbar Seroussi, and Moritz Helias. A unified approach to feature learning in bayesian neural networks. In *High-dimensional Learning Dynamics 2024: The Emergence of Structure and Reasoning*, 2024.
- [39] Alexander van Meegen and Haim Sompolinsky. Coding schemes in neural networks learning classification tasks, 2024.
- [40] Alessandro Inghrosso, Rosalba Pacelli, Pietro Rotondo, and Federica Gerace. Statistical mechanics of transfer learning in fully connected networks in the proportional limit. *Physical Review Letters*, 134(17):177301, 2025.
- [41] Haozhe Shan, Qianyi Li, and Haim Sompolinsky. Order parameters and phase transitions of continual learning in deep neural networks, 2025.
- [42] Javan Tahir, Surya Ganguli, and Grant M. Rotskoff. Features are fate: a theory of transfer learning in high-dimensional regression, 2024.
- [43] Jacopo Galdi, Giulia Lanzillotta, Lorenzo Noci, Benjamin F Grewe, and Thomas Hofmann. To learn or not to learn: Exploring the limits of feature learning in continual learning. In *NeurIPS 2024 Workshop on Scalable Continual Learning for Lifelong Foundation Models*, 2024.
- [44] Song Mei, Andrea Montanari, and Phan-Minh Nguyen. A mean field view of the landscape of two-layer neural networks. *Proceedings of the National Academy of Sciences*, 115(33):E7665–E7671, 2018.
- [45] Greg Yang and Edward J. Hu. Feature learning in infinite-width neural networks, 2022.

- [46] Grant Rotskoff and Eric Vanden-Eijnden. Trainability and accuracy of artificial neural networks: An interacting particle system approach. *Communications on Pure and Applied Mathematics*, 75(9):1889–1935, 2022.
- [47] Patrick Charbonneau, Enzo Marinari, Giorgio Parisi, Federico Ricci-terseghi, Gabriele Sicuro, Francesco Zamponi, and Marc Mezard. *Spin glass theory and far beyond: replica symmetry breaking after 40 years*. World Scientific, 2023.
- [48] Silvio Franz and Giorgio Parisi. Quasi-equilibrium in glassy dynamics: an algebraic view. *Journal of Statistical Mechanics: Theory and Experiment*, 2013(02):P02003, 2013.
- [49] Andrew M. Saxe, James L. McClelland, and Surya Ganguli. Exact solutions to the nonlinear dynamics of learning in deep linear neural networks, 2014.
- [50] Madhu S. Advani and Andrew M. Saxe. High-dimensional dynamics of generalization error in neural networks, 2017.
- [51] Arthur Jacot, François Ged, Berfin Şimşek, Clément Hongler, and Franck Gabriel. Saddle-to-saddle dynamics in deep linear networks: Small initialization training, symmetry, and sparsity, 2022.
- [52] Jacob A Zavatore-Veth, Abdulkadir Canatar, Benjamin S Ruben, and Cengiz Pehlevan. Asymptotics of representation learning in finite bayesian neural networks*. *Journal of Statistical Mechanics: Theory and Experiment*, 2022(11):114008, November 2022.
- [53] Nasim Rahaman, Aristide Baratin, Devansh Arpit, Felix Draxler, Min Lin, Fred A. Hamprecht, Yoshua Bengio, and Aaron Courville. On the spectral bias of neural networks, 2019.
- [54] Roman Novak, Yasaman Bahri, Daniel A. Abolafia, Jeffrey Pennington, and Jascha Sohl-Dickstein. Sensitivity and generalization in neural networks: an empirical study, 2018.
- [55] Mikhail Belkin, Daniel Hsu, Siyuan Ma, and Soumik Mandal. Reconciling modern machine-learning practice and the classical bias–variance trade-off. *Proceedings of the National Academy of Sciences*, 116(32):15849–15854, July 2019.
- [56] Zhi-Qin John Xu Zhi-Qin John Xu, Yaoyu Zhang Yaoyu Zhang, Tao Luo Tao Luo, Yanyang Xiao Yanyang Xiao, and Zheng Ma Zheng Ma. Frequency principle: Fourier analysis sheds light on deep neural networks. *Communications in Computational Physics*, 28(5):1746–1767, January 2020.
- [57] Yatin Dandi, Florent Krzakala, Bruno Loureiro, Luca Pesce, and Ludovic Stephan. How two-layer neural networks learn, one (giant) step at a time, 2023.
- [58] Emanuele Troiani, Yatin Dandi, Leonardo Defilippis, Lenka Zdeborová, Bruno Loureiro, and Florent Krzakala. Fundamental computational limits of weak learnability in high-dimensional multi-index models. *arXiv preprint arXiv:2405.15480*, 2024.
- [59] Yatin Dandi, Luca Pesce, Hugo Cui, Florent Krzakala, Yue M Lu, and Bruno Loureiro. A random matrix theory perspective on the spectrum of learned features and asymptotic generalization capabilities. *arXiv preprint arXiv:2410.18938*, 2024.
- [60] Emmanuel Abbe, Enric Boix-Adsera, Matthew Brennan, Guy Bresler, and Dheeraj Nagaraj. The staircase property: How hierarchical structure can guide deep learning, 2021.
- [61] Emmanuel Abbe, Enric Boix-Adsera, and Theodor Misiakiewicz. Sgd learning on neural networks: leap complexity and saddle-to-saddle dynamics, 2023.
- [62] Emmanuel Abbe, Enric Boix-Adsera, and Theodor Misiakiewicz. The merged-staircase property: a necessary and nearly sufficient condition for sgd learning of sparse functions on two-layer neural networks, 2024.
- [63] Jiang Yang, Yuxiang Zhao, and Quanhui Zhu. Effective rank and the staircase phenomenon: New insights into neural network training dynamics, 2025.

- [64] Alethea Power, Yuri Burda, Harri Edwards, Igor Babuschkin, and Vedant Misra. Grokking: Generalization beyond overfitting on small algorithmic datasets, 2022.
- [65] Ziming Liu, Ouail Kitouni, Niklas Nolte, Eric J. Michaud, Max Tegmark, and Mike Williams. Towards understanding grokking: An effective theory of representation learning, 2022.
- [66] Tanishq Kumar, Blake Bordelon, Samuel J. Gershman, and Cengiz Pehlevan. Grokking as the transition from lazy to rich training dynamics, 2024.
- [67] Simin Fan, Razvan Pascanu, and Martin Jaggi. Deep grokking: Would deep neural networks generalize better?, 2024.
- [68] Yamini Bansal, Gal Kaplun, and Boaz Barak. For self-supervised learning, rationality implies generalization, provably. In *International Conference on Learning Representations*, 2021.
- [69] Edward J Hu, Yelong Shen, Phillip Wallis, Zeyuan Allen-Zhu, Yuanzhi Li, Shean Wang, Lu Wang, Weizhu Chen, et al. Lora: Low-rank adaptation of large language models. *ICLR*, 1(2):3, 2022.
- [70] Yamini Bansal, Preetum Nakkiran, and Boaz Barak. Revisiting model stitching to compare neural representations. *Advances in neural information processing systems*, 34:225–236, 2021.
- [71] Blake Bordelon, Alexander Atanasov, and Cengiz Pehlevan. How feature learning can improve neural scaling laws, 2024.
- [72] Silvio Franz and Giorgio Parisi. Recipes for metastable states in spin glasses. *Journal de Physique I*, 5(11):1401–1415, November 1995.
- [73] Carlo Baldassi, Alessandro Ingrosso, Carlo Lucibello, Luca Saglietti, and Riccardo Zecchina. Subdominant dense clusters allow for simple learning and high computational performance in neural networks with discrete synapses. *Physical Review Letters*, 115(12), September 2015.
- [74] Carlo Baldassi, Christian Borgs, Jennifer T. Chayes, Alessandro Ingrosso, Carlo Lucibello, Luca Saglietti, and Riccardo Zecchina. Unreasonable effectiveness of learning neural networks: From accessible states and robust ensembles to basic algorithmic schemes. *Proceedings of the National Academy of Sciences*, 113(48):E7655–E7662, 2016.
- [75] Carlo Baldassi, Fabrizio Pittorino, and Riccardo Zecchina. Shaping the learning landscape in neural networks around wide flat minima. *Proceedings of the National Academy of Sciences*, 117(1):161–170, December 2019.
- [76] Carlo Baldassi, Clarissa Lauditi, Enrico M. Malatesta, Gabriele Perugini, and Riccardo Zecchina. Unveiling the structure of wide flat minima in neural networks. *Phys. Rev. Lett.*, 127:278301, Dec 2021.
- [77] Carlo Baldassi, Clarissa Lauditi, Enrico M. Malatesta, Rosalba Pacelli, Gabriele Perugini, and Riccardo Zecchina. Learning through atypical phase transitions in overparameterized neural networks. *Phys. Rev. E*, 106:014116, Jul 2022.

A Setting and related works for Bayesian NNs

In this section, we would like to study the effect of transfer learning for infinitely wide Bayesian neural networks. Here, we suppose that a two layer NN with parameters $\theta = \text{Vec}\{\mathbf{W}, \mathbf{w}\}$ has to learn a target task \mathcal{T}_2 composed of P_2 input-output pairs $\{\mathbf{x}_\mu, y_\mu\}_{\mu=1}^{P_2}$, where the input vector is $\mathbf{x}_\mu \in \mathbb{R}^D$, $\{D, P_2\} = \Theta_N(1)$ are fixed, and the network width N is going to infinity. The case where the solution space is sampled from a posterior that is a Gibbs distribution with generic log-likelihood $\mathcal{L}(\theta, \mathcal{T})$ and a Gaussian prior $\frac{1}{2}\|\theta\|^2$ has been studied in [14]. Here, the purpose is to integrate the effect of transfer learning from a source task \mathcal{T}_1 with the effect of feature learning on \mathcal{T}_2 .

We consider the weights $\bar{\theta} = \text{Vec}\{\bar{\mathbf{W}}, \bar{\mathbf{w}}\}$ of a pre-trained model on $\mathcal{T}_1 = \{\bar{\mathbf{x}}_\mu, \bar{y}_\mu\}_{\mu=1}^{P_1}$ as quenched disorder variables for the target task \mathcal{T}_2 , since these weights adapt only on \mathcal{T}_1 , while the target task variables are annealed $\theta = \text{Vec}\{\mathbf{W}, \mathbf{w}\}$. The quantity of interest we would like to compute is the free energy

$$\begin{aligned} \mathbb{E}_{\bar{\mathbf{W}} \sim p(\bar{\theta}|\mathcal{T}_1)} \mathcal{F}[\bar{\mathbf{W}}] &= - \lim_{N \rightarrow \infty} \frac{1}{N} \mathbb{E}_{\bar{\mathbf{W}} \sim p(\bar{\theta}|\mathcal{T}_1)} \ln Z[\bar{\mathbf{W}}] \\ &= - \lim_{N \rightarrow \infty} \frac{1}{N} \mathbb{E}_{\bar{\mathbf{W}} \sim p(\bar{\theta}|\mathcal{T}_1)} \ln \left[\int d\theta \exp \left(-\frac{\beta N \gamma_0^2}{2} \sum_{\mu=1}^{P_2} \mathcal{L}(\theta, \mathcal{T}_2) \right) - \frac{1}{2} \|\theta\|^2 - \frac{\delta}{2} \|\mathbf{W} - \bar{\mathbf{W}}\|^2 \right]. \end{aligned} \quad (14)$$

Here, the dependency on the source weights $\bar{\mathbf{W}} \in \mathbb{R}^{N \times D}$ appears through an elastic coupling δ that acts as a form of regularization for the target task weights $\mathbf{W} \in \mathbb{R}^{N \times D}$ of \mathcal{T}_2 . To guarantee that the source configuration effectively solved \mathcal{T}_1 , we take the expectation over the posterior distribution of the source weights as sampled from the Gibbs measure

$$p(\bar{\theta}|\mathcal{T}_1) = \frac{1}{\mathcal{Z}_1} \exp \left(-\frac{\beta N \bar{\gamma}_0^2}{2} \sum_{\mu=1}^{P_1} \mathcal{L}(\bar{\theta}, \mathcal{T}_1) - \frac{1}{2} \|\bar{\theta}\|^2 \right). \quad (15)$$

As clarified in the main text, both $\{\bar{\gamma}_0, \gamma_0\} = \Theta_N(1)$ in the mean-field parameterization act as richness parameters that tune the level of feature learning strength, respectively on \mathcal{T}_1 and \mathcal{T}_2 [26, 71, 14]. This is the reason why, in our theory, representation learning remains an $\Theta_N(1)$ effect at infinite width even when $P = \Theta_N(1)$, contrary to what would happen in the theories of [29, 30], whose infinitely overparameterized limit $\alpha = P/N \rightarrow 0$ recovers the NNGP lazy kernel at infinite width.

The way on constraining the target weights to the source weights through an elastic coupling as in Eq. (14) was first proposed by [40] in the context of transfer learning and then studied by [41] in the continual learning setting. The form of Eq. (14) is known in spin glasses literature under the name of Franz-Parisi potential [72], used to favor posterior weight around metastable minima in the energy landscape. In the context of machine learning theory, a line of works [73, 74, 75, 76, 77] focused on shallow architectures, made use of the Franz-Parisi potential in order to target subdominant flat regions of solutions in the loss landscape of a given task \mathcal{T} . Here, we stress that our theory of transfer learning described by Eq. (14), leads to different results than the theories of [40, 41]. The authors of [40, 41] focused on a proportional limit where both the size of the training sets (P_1, P_2 in our notation) and the width N go to infinity with some fixed ratios $\alpha_1 = P_1/N$ and $\alpha_2 = P_2/N$. The network parameterization they study is the standard NTK parameterization. In order to be able to study the proportional limit, they make a Gaussian Equivalence assumption for non-linear activation functions. Their theory predicts that, at finite α , the effect of transfer learning occurs due to a renormalization effect of a *fixed* source-target kernel, accordingly to the Bayesian theories of [29, 30]. More importantly, in the $\alpha \rightarrow 0$ overparameterized limit we are considering here, their theory predicts that TL has no effect on learning, since they recover the NNGP lazy kernel in this limit.

On the contrary, here we study the effect of mean-field (μP) parameterization to transfer learning in the overparameterized limit. As clarified by Eq. (14), we scale the likelihood by N in order to ensure we get a non-trivial contribution from the likelihood in the infinite width limit, and we scale the network readout with $\gamma_0 N$ (see Eq. (1)). The form of our posterior combined with the parameterization we choose allows us to get a theory of feature learning where kernels adapt to data in a non-trivial manner even when $P = \Theta_N(1)$. In fact, as clarified in [14], the posterior of Eq. (15) do not recover the NNGP lazy kernel, and the effect of transfer learning remains non-negligible

in our theory at finite P . Our theory do not require any Gaussian Equivalence assumptions on the pre-activation distribution. Indeed, as we clarify in Sec. 2.2, the combined effect of feature and transfer learning leads to non-Gaussian pre-activations. We get a set of saddle point equations for the kernels of both source (\mathcal{T}_1) and downstream (\mathcal{T}_2) tasks that have to be solved self-consistently. Thus, the kernels in our theory are not fixed but adapt to data, because representation learning shapes the pre-activation distribution, contrarily to what happens in the theories of [40, 41].

B Experimental Details

For Figures 10 and 2 we run discretized Langevin dynamics with $\beta = 50$ and step size $\eta = 0.001$. Langevin dynamics are run for $T = 200,000$ steps and convergence of the loss usually occurs around 50,000 steps. We compute averages of the losses and kernels over time after 50,000 steps. The theoretical equations for Φ , $\hat{\Phi}$ are solved directly with no need for Monte-carlo sampling since the network is linear.

For the nonlinear networks, we start the first layer weights at $\bar{\mathbf{W}}$, randomly reset the readout weights and run gradient descent (without Langevin noise) on both.

For CIFAR-10 plots on MLPs, we converted the image to grayscale, standardized the entries of the data, and downsampled it to be 28×28 to match the size of MNIST images. The classes are always balanced for any P_1, P_2 .

All experiments are performed on a Nvidia A100 GPU. The total net runtime of all exeriments takes about 6 hours.

C Theoretical Derivation of the Free Energy

Here, we proceed in reporting the actual computation of the free energy in Eq. (14). In order to compute the average over the source posterior we use the replica trick $\ln Z = \lim_{n \rightarrow 0} \frac{Z^n - 1}{n}$, and we introduce a set of n replicas $a \in \{n\}$ for the source weights $\{\mathbf{W}^a, \mathbf{w}^a\}$. As a consequence, we get

$$\begin{aligned} \mathbb{E}Z^n &= \int d\bar{\mathbf{W}} d\bar{\mathbf{w}} \prod_{a=1}^n d\mathbf{W}^a d\mathbf{w}^a d\bar{f}_\mu^a d\bar{f}_\mu^a \exp \left(-\frac{N\beta\gamma_0^2}{2} \sum_{\mu \in \mathcal{T}_1} [\bar{f}_\mu - \bar{y}_\mu]^2 - \frac{N\beta\gamma_0^2}{2} \sum_{a=1}^n \sum_{\mu \in \mathcal{T}_2} [f_\mu^a - y_\mu]^2 \right) \\ &\quad \exp \left(-\frac{1}{2} \sum_{a=1}^n |\mathbf{W}^a|^2 - \frac{1}{2} \sum_{a=1}^n |\mathbf{w}^a|^2 - \frac{1}{2} |\bar{\mathbf{w}}|^2 - \frac{1}{2} |\bar{\mathbf{W}}|^2 - \frac{\delta}{2} \sum_{a=1}^n |\mathbf{W}^a - \bar{\mathbf{W}}|^2 \right) \\ &\quad \int \prod_{a, \mu \in \mathcal{T}_1} d\hat{h}_\mu^a d\hat{h}_\mu^a \prod_{\mu \in \mathcal{T}_2} d\bar{h}_\mu d\hat{h}_\mu \exp \left(i \sum_{a=1}^n \sum_{\mu \in \mathcal{T}_2} \hat{h}_\mu^a \left(h_\mu^a - \frac{1}{\sqrt{D}} \mathbf{W}^a \mathbf{x}_\mu \right) + i \sum_{\mu \in \mathcal{T}_1} \hat{h}_\mu \left(\bar{h}_\mu - \frac{1}{\sqrt{D}} \bar{\mathbf{W}} \mathbf{x}_\mu \right) \right) \\ &\quad \int d\hat{f}_\mu^a d\hat{f}_\mu \exp \left(\sum_{a, \mu \in \mathcal{T}_2} \hat{f}_\mu^a (N\gamma_0 f_\mu^a - \mathbf{w}^a \cdot \phi(\mathbf{h}_\mu^a)) + \sum_{\mu \in \mathcal{T}_1} \hat{f}_\mu (N\gamma_0 \bar{f}_\mu - \bar{\mathbf{w}} \cdot \phi(\bar{\mathbf{h}}_\mu)) \right) \end{aligned} \quad (16)$$

Step 1. The first step consists in integrating out over \mathbf{W}^a and \mathbf{w}^a . We will write these as averages over a standard normal matrices (the prior)

$$\begin{aligned} \mathbb{E}_{\mathbf{W}^a \sim \mathcal{N}(0, (1+\delta)^{-1})} &\exp \left(\delta \mathbf{W}^a \cdot \bar{\mathbf{W}} - \frac{i}{\sqrt{D}} \sum_a \sum_{\mu \in \mathcal{T}_2} \hat{h}_\mu^a \mathbf{W}^a \mathbf{x}_\mu \right) \\ &= \exp \left(-\frac{1}{2(1+\delta)} \sum_{\mu, \nu \in \mathcal{T}_2} \hat{h}_\mu^a \cdot \hat{h}_\nu^a C_{\mu\nu} + \frac{\delta^2}{2(1+\delta)} |\bar{\mathbf{W}}|^2 - i \frac{\delta}{1+\delta} \sum_{\mu \in \mathcal{T}_2} \hat{h}_\mu^a \cdot \bar{\mathbf{h}}_\mu \right) \\ \mathbb{E}_{\mathbf{w}^a \sim \mathcal{N}(0, 1)} &\exp \left(-\sum_a \sum_{\mu \in \mathcal{T}_2} \hat{f}_\mu^a \phi(\mathbf{h}_\mu^a) \cdot \mathbf{w}^a \right) = \exp \left(\frac{N}{2} \sum_a \sum_{\mu, \nu \in \mathcal{T}_2} \hat{f}_\mu^a \hat{f}_\nu^a \Phi_{\mu\nu}^a \right). \end{aligned} \quad (17)$$

We see that we must introduce the kernels and their dual variables $\{\Phi_{\mu\nu}^a, \hat{\Phi}_{\mu\nu}\}_{\mu\nu \in \mathcal{T}_2, a \in \{n\}}$ as order parameters, but these are decoupled over replica index

$$\Phi_{\mu\nu}^a \equiv \frac{1}{N} \phi(\mathbf{h}_\mu^a) \cdot \phi(\mathbf{h}_\nu^a) \quad (18)$$

and enforce their definitions through some Dirac-delta functions

$$1 = \int d\Phi_{\mu\nu}^a \delta\left(\Phi_{\mu\nu}^a - \frac{1}{N} \phi(\mathbf{h}_\mu^a) \cdot \phi(\mathbf{h}_\nu^a)\right) = \int \frac{d\Phi_{\mu\nu}^a d\hat{\Phi}_{\mu\nu}^a}{2\pi} \exp\left(i\hat{\Phi}_{\mu\nu}^a \left(\Phi_{\mu\nu}^a - \frac{1}{N} \phi(\mathbf{h}_\mu^a) \cdot \phi(\mathbf{h}_\nu^a)\right)\right). \quad (19)$$

Step 2: integrate over $\bar{\mathbf{W}}$ and $\bar{\mathbf{w}}$

$$\begin{aligned} & \mathbb{E}_{\bar{\mathbf{W}}} \exp\left(-\frac{\delta n}{2} |\bar{\mathbf{W}}|^2 + \frac{\delta^2 n}{2(1+\delta)} |\bar{\mathbf{W}}|^2 - \frac{i}{\sqrt{D}} \sum_{\mu \in \mathcal{T}_1 \cup \mathcal{T}_2} \hat{\mathbf{h}}_\mu \bar{\mathbf{W}} \mathbf{x}_\mu\right) \\ & \sim_{n \rightarrow 0} \exp\left(-\frac{1}{2} \sum_{\mu\nu \in \mathcal{T}_1 \cup \mathcal{T}_2} C_{\mu\nu} \hat{\mathbf{h}}_\mu \cdot \hat{\mathbf{h}}_\nu\right) \\ & \mathbb{E}_{\bar{\mathbf{w}} \sim \mathcal{N}(0,1)} \exp\left(-\sum_{\mu \in \mathcal{T}_1} \hat{f}_\mu \phi(\mathbf{h}_\mu) \cdot \bar{\mathbf{w}}\right) = \exp\left(\frac{N}{2} \sum_{\mu, \nu \in \mathcal{T}_1} \hat{f}_\mu \hat{f}_\nu \bar{\Phi}_{\mu\nu}\right) \end{aligned} \quad (20)$$

Here, similarly as we did in Eq. (18), we enforce the definitions of the source task kernels $\{\bar{\Phi}_{\mu\nu}, \hat{\bar{\Phi}}_{\mu\nu}\}_{\mu\nu \in \mathcal{T}_1}$, which do not carry any replica index.

Step 3: Factorize everything across the N hidden neurons

$$\begin{aligned} \langle Z^n \rangle & \propto \int d\bar{\Phi} d\hat{\bar{\Phi}} d\bar{f}_\mu d\hat{\bar{f}}_\mu \prod_{a=1}^n d\Phi^a d\hat{\Phi}^a d f^a d \hat{f}^a \exp\left(-\frac{\beta N \bar{\gamma}_0^2}{2} \sum_{\mu \in \mathcal{T}_1} [\bar{f}_\mu - y_\mu]^2 - \frac{\beta N \gamma_0^2}{2} \sum_a \sum_{\mu \in \mathcal{T}_2} [f_\mu^a - y_\mu]^2\right) \\ & \exp\left(N\gamma_0 \sum_{\mu a} \hat{f}_\mu^a f_\mu^a + N\bar{\gamma}_0 \sum_{\mu} \hat{\bar{f}}_\mu \bar{f}_\mu + \frac{N}{2} \sum_{a\mu\nu} \hat{\Phi}_{\mu\nu}^a \Phi_{\mu\nu}^a + \frac{N}{2} \sum_{\mu\nu} \bar{\Phi}_{\mu\nu} \hat{\bar{\Phi}}_{\mu\nu}\right) \\ & \exp\left(\frac{N}{2} \sum_{a\mu\nu} \hat{f}_\mu^a \hat{f}_\nu^a \Phi_{\mu\nu}^a + \frac{N}{2} \sum_{\mu\nu} \hat{\bar{f}}_\mu \hat{\bar{f}}_\nu \bar{\Phi}_{\mu\nu} + N \ln \mathcal{Z}_{joint}\right) \end{aligned} \quad (21)$$

where \mathcal{Z}_{joint} is the joint single-site density that carries contributions from both \mathcal{T}_1 and \mathcal{T}_2 . It has the form

$$\begin{aligned} \mathcal{Z}_{joint} & = \int d h_\mu^a d \hat{h}_\mu^a d \bar{h}_\mu d \hat{\bar{h}}_\mu \exp\left(-\frac{1}{2(1+\delta)} \sum_{a\mu\nu \in \mathcal{T}_2} \hat{h}_\mu^a \hat{h}_\nu^a C_{\mu\nu} - \frac{1}{2} \sum_{a\mu\nu} \phi(h_\mu^a) \phi(h_\nu^a) \hat{\bar{\Phi}}_{\mu\nu}^a\right) \\ & \exp\left(-\frac{1}{2} \sum_{\mu\nu \in \mathcal{T}_1 \cup \mathcal{T}_2} \hat{\bar{h}}_\mu \hat{\bar{h}}_\nu C_{\mu\nu} - \frac{1}{2} \sum_{\mu\nu} \phi(\bar{h}_\mu) \phi(\bar{h}_\nu) \hat{\bar{\Phi}}_{\mu\nu} - i \frac{\delta}{1+\delta} \sum_{a\mu} \bar{h}_\mu \hat{h}_\mu^a\right) \\ & \exp\left(i \sum_{a\mu} \hat{h}_\mu^a h_\mu^a + i \sum_{\mu} \hat{\bar{h}}_\mu \bar{h}_\mu\right). \end{aligned} \quad (22)$$

Notice that, if $\delta = 0$ in Eq. (22), the single site densities on \mathcal{T}_1 and \mathcal{T}_2 are perfectly decoupled as it should be, since no transfer learning effect would come into play. Instead, as soon as we keep $\delta > 0$, there is an interaction between the fields of the source task $\bar{\mathbf{h}}$ and the dual fields of the target task $\hat{\mathbf{h}}^a$ that will modify the $p(\mathbf{h}^a)$ distribution as we show in the next section.

C.1 RS Ansatz

Step 3: Staring at these equations the only solution that makes sense is the Replica-Symmetric solution $\Phi^a = \Phi$ and $f^a = f$. Plugging this ansatz into the expressions and taking the $n \rightarrow 0$ limit,

we get

$$\begin{aligned}\ln \mathcal{Z}_{joint} &= \ln \int d\bar{h}d\hat{h} \exp \left(-\frac{1}{2} \sum_{\mu\nu \in \mathcal{T}_1 \cup \mathcal{T}_2} \hat{h}_\mu \hat{h}_\nu C_{\mu\nu} - \frac{1}{2} \sum_{\mu\nu \in \mathcal{T}_1} \phi(\bar{h}_\mu) \phi(\bar{h}_\nu) \hat{\Phi}_{\mu\nu} + i \sum_{\mu \in \mathcal{T}_1 \cup \mathcal{T}_2} \hat{h}_\mu \bar{h}_\mu \right) \\ &\quad \times \exp(n \ln \mathcal{Z}_2[\bar{h}]) \\ &= \ln \mathcal{Z}_1 + \ln [1 + n \langle \ln \mathcal{Z}_2[\bar{h}] \rangle_1] \sim \ln \mathcal{Z}_1 + n \langle \ln \mathcal{Z}_2[\bar{h}] \rangle_1\end{aligned}$$

where $\ln \mathcal{Z}_2$ is the single site density for task \mathcal{T}_2

$$\begin{aligned}\mathcal{Z}_2[\bar{h}] &= \int dh_\mu d\hat{h}_\mu \exp \left(-\frac{1}{2(1+\delta)} \sum_{\mu\nu \in \mathcal{T}_2} \hat{h}_\mu \hat{h}_\nu C_{\mu\nu} - \frac{1}{2} \sum_{\mu\nu \in \mathcal{T}_2} \phi(h_\mu) \phi(h_\nu) \hat{\Phi}_{\mu\nu} \right) \\ &\quad \times \exp \left(i \sum_{\mu} \hat{h}_\mu h_\mu - i \frac{\delta}{1+\delta} \sum_{\mu} \bar{h}_\mu \hat{h}_\mu \right) \\ &= \int dh_\mu \exp \left(-\frac{(1+\delta)}{2} \sum_{\mu\nu} \left(h_\mu - \frac{\delta}{1+\delta} \bar{h}_\mu \right) C_{\mu\nu}^{-1} \left(h_\nu - \frac{\delta}{1+\delta} \bar{h}_\nu \right) - \frac{1}{2} \sum_{\mu\nu \in \mathcal{T}_2} \phi(h_\mu) \phi(h_\nu) \hat{\Phi}_{\mu\nu} \right).\end{aligned}$$

Again, if $\delta = 0$, there would be no dependency on the source task \mathcal{T}_1 in Eq. (23). We stress that transfer learning has the effect of shifting and scaling all the moments of the distribution $p(\mathbf{h})$ towards $p(\bar{\mathbf{h}})$ as δ becomes larger and larger, while feature learning effect on Eq. (23) appear through the contribution of the non-Gaussian exponent proportional to the dual kernel $\hat{\Phi}$.

C.2 Saddle point equations

In the infinite width $N \rightarrow \infty$ limit the replicated action of Eq. (21) is dominated by the set of kernels $\{\bar{\Phi}, \hat{\Phi}\} \in \mathcal{T}_1$ and $\{\Phi, \hat{\Phi}\} \in \mathcal{T}_2$ that makes the action S locally stationary ($\delta S = 0$)

$$\begin{aligned}\langle Z^n \rangle &= \int d\bar{\Phi} d\hat{\Phi} d\bar{f} d\hat{f} \exp \left(N S_1(\{\bar{\Phi}, \hat{\Phi}\}) \right) \left[\int d\Phi d\hat{\Phi} d f d\hat{f} \exp \left(N S_2(\{\Phi, \hat{\Phi}\}) \right) \right]^n \\ S_1 &= \frac{1}{2} \sum_{\mu\nu} \hat{\Phi}_{\mu\nu} \bar{\Phi}_{\mu\nu} + \frac{1}{2} \sum_{\mu\nu} \hat{f}_\mu \hat{f}_\nu \bar{\Phi}_{\mu\nu} + \bar{\gamma}_0 \sum_{\mu} \hat{f}_\mu \bar{f}_\mu - \frac{\beta \bar{\gamma}_0^2}{2} \sum_{\mu} [\bar{f}_\mu - \bar{y}_\mu]^2 + \ln \mathcal{Z}_1 \\ \mathcal{Z}_1 &= \int d\bar{h}_\mu d\hat{h}_\mu \exp \left(-\frac{1}{2} \sum_{\mu\nu} \hat{\Phi}_{\mu\nu} \phi(\bar{h}_\mu) \phi(\bar{h}_\nu) - \frac{1}{2} \sum_{\mu\nu} \hat{h}_\mu \hat{h}_\nu C_{\mu\nu} + i \sum_{\mu} \hat{h}_\mu \bar{h}_\mu \right) \\ S_2 &= \gamma_0 \sum_{\mu} f_\mu \hat{f}_\mu + \frac{1}{2} \sum_{\mu\nu} \hat{f}_\mu \hat{f}_\nu \Phi_{\mu\nu} - \frac{\beta \gamma_0^2}{2} \sum_{\mu} [f_\mu - y_\mu]^2 + \frac{1}{2} \sum_{\mu\nu} \hat{\Phi}_{\mu\nu} \Phi_{\mu\nu} + \langle \ln \mathcal{Z}_2[\bar{h}] \rangle_1 \\ \mathcal{Z}_2 &= \int dh_\mu d\hat{h}_\mu \exp \left(-\frac{1}{2(1+\delta)} \hat{h}_\mu \hat{h}_\nu C_{\mu\nu} - \frac{1}{2} \sum_{\mu\nu} \hat{\Phi}_{\mu\nu} \phi(h_\mu) \phi(h_\nu) + i \sum_{\mu} \hat{h}_\mu (h_\mu - \delta(1+\delta)^{-1} \bar{h}_\mu) \right).\end{aligned}\tag{23}$$

From these definitions, the saddle point equations give

$$\begin{aligned}
\frac{\partial S}{\partial \hat{\Phi}} &= \frac{1}{2} \bar{\Phi} - \frac{1}{2} \langle \phi(\bar{h}) \phi(\bar{h}) \rangle_1 + \mathcal{O}(n) \\
\frac{\partial S}{\partial \hat{\Phi}} &= \frac{1}{2} \Phi_{\mu\nu} - \frac{1}{2} \left\langle \langle \phi(h_\mu) \phi(h_\nu) \rangle_{|\bar{h}} \right\rangle_{\bar{h}} = 0 \\
\frac{\partial S}{\partial f_\mu} &= \gamma_0 \hat{f}_\mu - \beta \gamma_0^2 [f_\mu - y_\mu] = 0 \\
\frac{\partial S}{\partial \hat{f}_\mu} &= \sum_\nu \Phi_{\mu\nu} \hat{f}_\nu + \gamma_0 f_\mu = 0 \\
\frac{\partial S}{\partial \Phi} &= \hat{\Phi}_{\mu\nu} + \frac{1}{2} \hat{f}_\mu \hat{f}_\nu = 0
\end{aligned} \tag{24}$$

C.3 Regression tasks

These equations are generic for any loss function $\mathcal{L}(\boldsymbol{\theta}, \mathcal{T})$. In the following, for simplicity, we will specialize to regression problems where $\mathcal{L}(\boldsymbol{\theta}, \mathcal{T}) = \frac{1}{2} \sum_{\mu=1}^P (f_\mu - y_\mu)^2$ for both source and target tasks. In this particular case, one can solve for both $\{\hat{f}_\mu, \hat{f}_\mu\}$ and $\{f_\mu, \hat{f}_\mu\}$ explicitly, since the squared-error loss (SE) allows to integrate out the last layer readouts. From that, one gets for the dual source and target kernels

$$\begin{aligned}
\hat{\Phi} &= -\bar{\gamma}_0^2 \left(\frac{\mathbf{I}}{\beta} + \bar{\Phi} \right)^{-1} \bar{\mathbf{y}} \bar{\mathbf{y}}^\top \left(\frac{\mathbf{I}}{\beta} + \bar{\Phi} \right)^{-1} \\
\hat{\Phi} &= -\gamma_0^2 \left(\frac{\mathbf{I}}{\beta} + \Phi \right)^{-1} \mathbf{y} \mathbf{y}^\top \left(\frac{\mathbf{I}}{\beta} + \Phi \right)^{-1}.
\end{aligned} \tag{25}$$

Notice that the two equations are functionally equivalent, but what changes is the dependency on different task labels $\{\bar{\mathbf{y}}\} \in \mathcal{T}_1$ vs $\{\mathbf{y}\} \in \mathcal{T}_2$, different levels of feature learning strength in principle $\{\bar{\gamma}_0, \gamma_0\}$, and especially different adaptive kernels $\bar{\Phi}$ vs Φ .

C.4 Generalization Error

Knowing the form of the transfer free energy of Eq. (14), makes it easy to compute the test error of the target model on a new (unseen) example (\mathbf{x}_0, y_0) . For a generic loss, this is defined as

$$\epsilon_g(\mathbf{x}_0, y_0) = \mathbb{E}_{\bar{\mathbf{W}} \sim p(\bar{\boldsymbol{\theta}}|\mathcal{T}_1)} \langle \mathcal{L}(\boldsymbol{\theta}; \{\mathbf{x}_0, y_0\}) \rangle_{\boldsymbol{\theta} \sim p(\boldsymbol{\theta}|\mathcal{T}_2, \bar{\mathbf{W}})} \tag{26}$$

and can be easily computed by realizing that, if we introduce a ‘‘test-point coupling’’ ϵ into the transfer free energy by adding a weighted loss for the unseen sample (\mathbf{x}_0, y_0) , we get an extended free energy

$$\begin{aligned}
\mathcal{F}(\epsilon) &= - \lim_{N \rightarrow \infty} \frac{1}{N} \mathbb{E}_{\bar{\mathbf{W}} \sim p(\bar{\boldsymbol{\theta}}|\mathcal{T}_1)} \ln \int d\boldsymbol{\theta} \exp \left(-\frac{\beta N \gamma_0^2}{2} \left(\sum_{\mu \in \mathcal{T}_2} \mathcal{L}(\boldsymbol{\theta}; \mathcal{T}_2) + \epsilon \mathcal{L}(\boldsymbol{\theta}; \{\mathbf{x}_0, y_0\}) \right) \right) \\
&\quad \times \exp \left(-\frac{1}{2} \|\boldsymbol{\theta}\|^2 - \frac{\delta}{2} \|\mathbf{W} - \bar{\mathbf{W}}\|^2 \right)
\end{aligned}$$

from which the test loss can be easily computed as

$$\epsilon_g = \frac{2}{\beta \gamma_0^2} \left. \frac{\partial \mathcal{F}(\epsilon)}{\partial \epsilon} \right|_{\epsilon=0}. \tag{27}$$

For regression task and SE loss, consistently with [14], this gives the kernel predictor

$$\epsilon_g(\mathbf{x}_0, y_0) = \left(y_0 - \sum_{\mu\nu} \Phi_{0\mu} \left[\Phi_{\mu\nu} + \frac{\mathbb{I}_{\mu\nu}}{\beta} \right]^{-1} y_\nu \right)^2 \tag{28}$$

being $\Phi_{0\mathcal{T}_2}$ the train-test kernel from the saddle point equation

$$\Phi_{0\mu} = \left\langle \langle \phi(h_0) \phi(h_\mu) \rangle_{|\{\bar{h}_0, \bar{h}\}} \right\rangle_{\{\bar{h}_0, \bar{h}\}} \tag{29}$$

similarly to Eq. (24) for the train kernel. We explicitly derive the close form of the train-test kernel for linear networks in the following Sec. C.5.

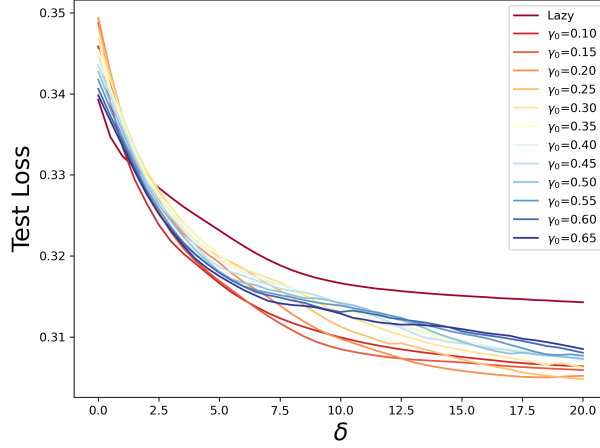


Figure 7: Langevin simulations of a $N = 20000$ two-layer ReLU network as a function of δ and for different feature learning strength values γ_0 . Test loss at convergence: the network is trained for 10^5 and averaged after $t = 5 \times 10^4$ every 10^3 steps. Lazy learning are smallest benefit from transfer learning. Optimal intermediate value of γ_0 .

C.5 Linear Networks

If we specialize to linear networks where $\phi(h) \equiv h$ and to regression tasks, the target action can be solved explicitly. Indeed, this is given by

$$S_2 = -\frac{1}{2} \sum_{\mu\nu} \Phi_{\mu\nu} \hat{\Phi}_{\mu\nu} + \frac{\gamma_0^2}{2} \mathbf{y}^\top \left(\Phi + \frac{\mathbf{I}}{\beta} \right)^{-1} \mathbf{y} - \langle \ln \mathcal{Z}_2[\bar{\mathbf{h}}] \rangle_1 \quad (30)$$

where the single-site remains now Gaussian even after feature learning, being

$$\mathcal{Z}_2 = \int d\mathbf{h}_\mu d\hat{\mathbf{h}}_\mu \exp \left(-\frac{1}{2(1+\delta)} \hat{\mathbf{h}}_\mu \hat{\mathbf{h}}_\nu C_{\mu\nu} - \frac{1}{2} \sum_{\mu\nu} \hat{\Phi}_{\mu\nu} h_\mu h_\nu + i \sum_{\mu} \hat{h}_\mu (h_\mu - \delta(1+\delta)^{-1} \bar{h}_\mu) \right). \quad (31)$$

Here, we can think $\hat{\mathbf{h}}, \mathbf{h}$ as jointly Gaussian with

$$\begin{bmatrix} \hat{\mathbf{h}} \\ \mathbf{h} \end{bmatrix} \sim \mathcal{N}(\boldsymbol{\mu}, \boldsymbol{\Sigma})$$

$$\boldsymbol{\mu} = \begin{bmatrix} (1+\delta)^{-1} \mathbf{C} & -i\mathbf{I} \\ -i\mathbf{I} & \hat{\Phi} \end{bmatrix}^{-1} \begin{bmatrix} -i\delta(1+\delta)^{-1} \bar{\mathbf{h}} \\ \mathbf{0} \end{bmatrix}, \quad \boldsymbol{\Sigma} = \begin{bmatrix} (1+\delta)^{-1} \mathbf{C} & -i\mathbf{I} \\ -i\mathbf{I} & \hat{\Phi} \end{bmatrix}^{-1}.$$

The mean and covariance are equal to

$$\langle \mathbf{h} \rangle_{|\bar{\mathbf{h}}} = \delta \left[(1+\delta) \mathbf{C}^{-1} + \hat{\Phi} \right]^{-1} \mathbf{C}^{-1} \bar{\mathbf{h}}, \quad \text{Cov}_{|\bar{\mathbf{h}}}(\mathbf{h}) = \left[(1+\delta) \mathbf{C}^{-1} + \hat{\Phi} \right]^{-1}. \quad (32)$$

We can thus compute the correlation of $\mathbf{h}|\bar{\mathbf{h}}$ as $\langle \mathbf{h} \mathbf{h}^\top \rangle = \langle \mathbf{h} \rangle \langle \mathbf{h} \rangle^\top + \text{Cov}(\mathbf{h})$

$$\langle \mathbf{h} \mathbf{h}^\top \rangle_{|\bar{\mathbf{h}}} = \left[(1+\delta) \mathbf{C}^{-1} + \hat{\Phi} \right]^{-1} + \delta^2 \left[(1+\delta) \mathbf{C}^{-1} + \hat{\Phi} \right]^{-1} \mathbf{C}^{-1} \bar{\mathbf{h}}_{\mathcal{T}_2} \bar{\mathbf{h}}_{\mathcal{T}_2}^\top \mathbf{C}^{-1} \left[(1+\delta) \mathbf{C}^{-1} + \hat{\Phi} \right]^{-1}. \quad (33)$$

Now, we must perform the covariance of $\bar{\mathbf{h}}$ using \mathcal{Z}_1 . Note that this is technically $\bar{\mathbf{h}}$ restricted to the second dataset \mathcal{T}_2 . The full covariance of $\bar{\mathbf{h}}$ for both $\mathcal{T}_1 \cup \mathcal{T}_2$ has the structure

$$\langle \bar{\mathbf{h}} \bar{\mathbf{h}}^\top \rangle = \left[\mathbf{C}_{\mathcal{T}_1 \cup \mathcal{T}_2}^{-1} + \begin{bmatrix} \hat{\Phi} & \mathbf{0} \\ \mathbf{0} & \mathbf{0} \end{bmatrix} \right]^{-1} = \mathbf{C}_{\mathcal{T}_1 \cup \mathcal{T}_2} \left[\mathbf{I} + \begin{bmatrix} \hat{\Phi} & \mathbf{0} \\ \mathbf{0} & \mathbf{0} \end{bmatrix} \mathbf{C}_{\mathcal{T}_1 \cup \mathcal{T}_2} \right]^{-1}. \quad (34)$$

We are interested in the lower (2, 2) block of this matrix, which gives the Schur complement

$$\langle \bar{\mathbf{h}}_{\mathcal{T}_2} \bar{\mathbf{h}}_{\mathcal{T}_2}^\top \rangle = \left[[\mathbf{C}^{-1}]_{22} - [\mathbf{C}^{-1}]_{21} \left([\mathbf{C}^{-1}]_{11} + \hat{\Phi} \right)^{-1} [\mathbf{C}^{-1}]_{12} \right]^{-1}. \quad (35)$$

Thus we are left with the final equations for the target kernels

$$\begin{aligned} \Phi &= \left[(1 + \delta) \mathbf{C}_{\mathcal{T}_2}^{-1} + \hat{\Phi} \right]^{-1} \\ &+ \delta^2 \left[(1 + \delta) \mathbf{C}_{\mathcal{T}_2}^{-1} + \hat{\Phi} \right]^{-1} \mathbf{C}_{\mathcal{T}_2}^{-1} \left[[\mathbf{C}^{-1}]_{22} - [\mathbf{C}^{-1}]_{21} \left([\mathbf{C}^{-1}]_{11} + \hat{\Phi} \right)^{-1} [\mathbf{C}^{-1}]_{12} \right]^{-1} \mathbf{C}_{\mathcal{T}_2}^{-1} \left[(1 + \delta) \mathbf{C}_{\mathcal{T}_2}^{-1} + \hat{\Phi} \right]^{-1} \end{aligned} \quad (36)$$

$$\hat{\Phi} = -\gamma_0^2 (\Phi + \beta^{-1} \mathbf{I})^{-1} \mathbf{y} \mathbf{y}^\top (\Phi + \beta^{-1} \mathbf{I})^{-1} \quad (37)$$

being the action

$$\begin{aligned} S_2 &= -\frac{1}{2} \text{Tr}(\Phi \hat{\Phi}) + \frac{\gamma_0^2}{2} \mathbf{y}^\top \left(\Phi + \frac{\mathbf{I}}{\beta} \right)^{-1} \mathbf{y} + \frac{1}{2} \ln \det \left[\mathbf{I} + \left(\frac{\mathbf{C}_{\mathcal{T}_2}}{1 + \delta} \right) \hat{\Phi} \right] \\ &- \frac{\delta^2}{2} \text{Tr} \left(\left[(\mathbf{C}_{\mathcal{T}_2})^{-1} \left[(1 + \delta) (\mathbf{C}_{\mathcal{T}_2})^{-1} + \hat{\Phi} \right]^{-1} (\mathbf{C}_{\mathcal{T}_2})^{-1} \right] \left[\langle \bar{\mathbf{h}}_{\mathcal{T}_2} \bar{\mathbf{h}}_{\mathcal{T}_2}^\top \rangle \right] \right). \end{aligned}$$

The saddle point equations for the source kernels were firstly derived in [14] and are instead

$$\begin{aligned} \bar{\Phi} &= \left[\mathbf{C}_{\mathcal{T}_1}^{-1} + \hat{\Phi} \right]^{-1} \\ \hat{\Phi} &= -\gamma_0^2 (\bar{\Phi} + \beta^{-1} \mathbf{I})^{-1} \bar{\mathbf{y}} \bar{\mathbf{y}}^\top (\bar{\Phi} + \beta^{-1} \mathbf{I})^{-1}. \end{aligned} \quad (38)$$

C.5.1 Train-Test adaptive kernels

In order to compute the test-train kernel to get the network predictor in the linear case, we need to compute $\Phi_{0T} = \langle \mathbf{h}_0 \mathbf{h}^\top \rangle = \langle \mathbf{h}_0 \rangle \langle \mathbf{h}^\top \rangle + \text{Cov}(\mathbf{h}_0, \mathbf{h}^\top)$. The covariance is computed by resorting to the single site extended to the test point with index 0

$$\mathcal{Z}_2[\bar{\mathbf{h}}] \propto \int \prod_{\mu=0}^{P_2} d h_\mu \exp \left(-\frac{1}{2} \sum_{\mu\nu=0}^{P_2} \left(h_\mu - \frac{\eta}{1 + \eta} \bar{h}_\mu \right) \left(\frac{\mathbf{C}_{\mu\nu}}{1 + \eta} \right)^{-1} \left(h_\nu - \frac{\eta}{1 + \eta} \bar{h}_\nu \right) - \frac{1}{2} \sum_{\mu\nu=1}^{P_2} h_\mu h_\nu \hat{\Phi}_{\mu\nu} \right) \quad (39)$$

from which

$$\left[\Lambda = \left((1 + \eta) \mathbf{C}^{-1} + \begin{pmatrix} 0 & 0 \\ 0 & \hat{\Phi} \end{pmatrix} \right)^{-1} \right] \quad (40)$$

and $\text{Cov}(\mathbf{h}_0, \mathbf{h}^\top) = \Lambda_{0T}$. It remains to compute

$$\begin{pmatrix} \langle \mathbf{h}_0 \rangle_{\cdot|\bar{\mathbf{h}}} \\ \langle \mathbf{h} \rangle_{\cdot|\bar{\mathbf{h}}} \end{pmatrix} = \eta \begin{pmatrix} \Lambda_{00} (\mathbf{C}_{00}^{-1} \bar{\mathbf{h}}_0 + \mathbf{C}_{0T}^{-1} \bar{\mathbf{h}}) + \Lambda_{0T} (\mathbf{C}_{T0}^{-1} \bar{\mathbf{h}}_0 + \mathbf{C}_{TT}^{-1} \bar{\mathbf{h}}) \\ \Lambda_{T0} (\mathbf{C}_{00}^{-1} \bar{\mathbf{h}}_0 + \mathbf{C}_{0T}^{-1} \bar{\mathbf{h}}) + \Lambda_{TT} (\mathbf{C}_{T0}^{-1} \bar{\mathbf{h}}_0 + \mathbf{C}_{TT}^{-1} \bar{\mathbf{h}}) \end{pmatrix} \quad (41)$$

where the subscript 0 refers to the test point while T to the training points $P_2 \in \mathcal{T}_2$. From Eq. ? we get

$$\begin{aligned} \langle \mathbf{h}_0 \rangle_{\cdot|\bar{\mathbf{h}}} \langle \mathbf{h}^\top \rangle_{\cdot|\bar{\mathbf{h}}} &= \eta^2 \Lambda_{00} \left(\mathbf{C}_{00}^{-1} \bar{\mathbf{h}}_0 \bar{\mathbf{h}}_0^\top \mathbf{C}_{00}^{-1} + \mathbf{C}_{00}^{-1} \bar{\mathbf{h}}_0 \bar{\mathbf{h}}^\top \mathbf{C}_{T0}^{-1} + \mathbf{C}_{0T}^{-1} \bar{\mathbf{h}} \bar{\mathbf{h}}_0^\top \mathbf{C}_{00}^{-1} + \mathbf{C}_{0T}^{-1} \bar{\mathbf{h}} \bar{\mathbf{h}}^\top \mathbf{C}_{T0}^{-1} \right) \Lambda_{0T} \\ &+ \eta^2 \Lambda_{00} \left(\mathbf{C}_{00}^{-1} \bar{\mathbf{h}}_0 \bar{\mathbf{h}}_0^\top \mathbf{C}_{0T}^{-1} + \mathbf{C}_{00}^{-1} \bar{\mathbf{h}}_0 \bar{\mathbf{h}}^\top \mathbf{C}_{TT}^{-1} + \mathbf{C}_{0T}^{-1} \bar{\mathbf{h}} \bar{\mathbf{h}}_0^\top \mathbf{C}_{0T}^{-1} + \mathbf{C}_{0T}^{-1} \bar{\mathbf{h}} \bar{\mathbf{h}}^\top \mathbf{C}_{TT}^{-1} \right) \Lambda_{TT} \\ &+ \eta^2 \Lambda_{0T} \left(\mathbf{C}_{T0}^{-1} \bar{\mathbf{h}}_0 \bar{\mathbf{h}}_0^\top \mathbf{C}_{00}^{-1} + \mathbf{C}_{T0}^{-1} \bar{\mathbf{h}}_0 \bar{\mathbf{h}}^\top \mathbf{C}_{T0}^{-1} + \mathbf{C}_{TT}^{-1} \bar{\mathbf{h}} \bar{\mathbf{h}}_0^\top \mathbf{C}_{00}^{-1} + \mathbf{C}_{TT}^{-1} \bar{\mathbf{h}} \bar{\mathbf{h}}^\top \mathbf{C}_{T0}^{-1} \right) \Lambda_{0T} \\ &+ \eta^2 \Lambda_{0T} \left(\mathbf{C}_{T0}^{-1} \bar{\mathbf{h}}_0 \bar{\mathbf{h}}_0^\top \mathbf{C}_{0T}^{-1} + \mathbf{C}_{T0}^{-1} \bar{\mathbf{h}}_0 \bar{\mathbf{h}}^\top \mathbf{C}_{TT}^{-1} + \mathbf{C}_{TT}^{-1} \bar{\mathbf{h}} \bar{\mathbf{h}}_0^\top \mathbf{C}_{0T}^{-1} + \mathbf{C}_{TT}^{-1} \bar{\mathbf{h}} \bar{\mathbf{h}}^\top \mathbf{C}_{TT}^{-1} \right) \Lambda_{TT}. \end{aligned} \quad (42)$$

As we did for the train kernels in the previous section, we are now interested in the lower (2, 2) block of each kernel matrix $\langle \bar{\mathbf{h}} \bar{\mathbf{h}}^\top \rangle_{\mathcal{T}_2}$ in Eq. (42), which would give the source kernel predictions of train and test kernels on \mathcal{T}_2 , having learned the source task \mathcal{T}_1 .

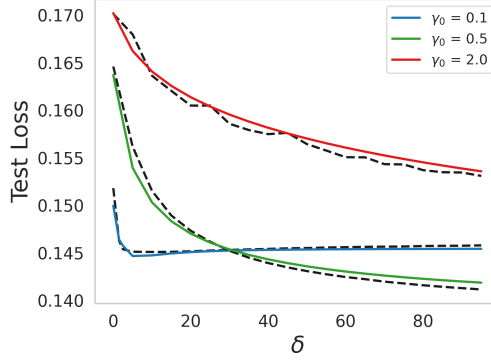


Figure 8: Test losses as a function of the elastic constraint η . Source task is a regression on two classes (0/1) of MNIST with $P_1 = 400$ labels $\bar{y} \in \{-1, 1\}^{P_1}$ and richness $\bar{\gamma}_0 = 0.5$. Target task is a regression on two classes of Fashion MNIST (2/5) with $P_2 = 50$ data points and labels $y \in \{-1, 1\}^{P_2}$ for different γ_0 .

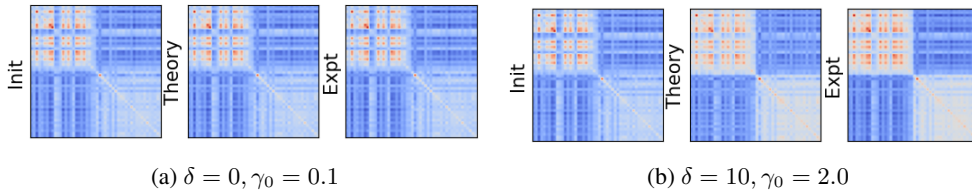


Figure 9: Kernels clustered by labels $y = \{\pm 1\}^{P_2}$ ($P_2 = 50$ Fashion-MNIST data from classes 2/5) improve their task alignment with $\delta > 0$ and high γ_0 . "Init" represents the Gram matrix of data, "Theory" and "Expt" refers to the adaptive feature kernels Φ .

In this setting, studying the test loss as given by Sec. C.4 as a function of δ requires to iteratively solve the saddle point equations (38) after having the adaptive source kernel values $\{\bar{\Phi}, \hat{\Phi}\} \in \mathcal{T}_1$. Fig. 7 shows that, depending on the feature strength γ_0 value on \mathcal{T}_2 , transfer learning advantage and so the dependency of test loss to δ may vary. When γ_0 is small and the target network is almost lazy on \mathcal{T}_2 , transfer learning has a minor effect in improving the test performance. There exists some optimal values of feature learning strength γ_0 and δ (which tunes how much the target network relies on source task features) which optimizes the network performance. In Fig. 9 we clearly show how the clustering of data points by labels pops out in the kernel appearance as soon as we both tune γ_0 and δ .

C.5.2 Decoupled $C_{\mathcal{T}_1 \cup \mathcal{T}_2}$

A special case we can study is the one in which data are whitened, and uncorrelated across both source and target tasks, meaning

$$C_{\mathcal{T}_1 \cup \mathcal{T}_2} = \begin{bmatrix} \mathbf{I} & \mathbf{0} \\ \mathbf{0} & \mathbf{I} \end{bmatrix} \quad (43)$$

In this case, we have

$$\langle \bar{h} \bar{h}^\top \rangle = \mathbf{I} \quad (44)$$

which simplifies the kernel saddle points on target task as

$$\begin{aligned} \Phi &= \left[(1 + \delta) \mathbf{I} + \hat{\Phi} \right]^{-1} + \delta^2 \left[(1 + \delta) \mathbf{I} + \hat{\Phi} \right]^{-2} \\ \hat{\Phi} &= -\gamma_0^2 (\Phi + \beta^{-1} \mathbf{I})^{-1} \mathbf{y} \mathbf{y}^\top (\Phi + \beta^{-1} \mathbf{I})^{-1}. \end{aligned} \quad (45)$$

As mentioned in the main text, since in this case the kernel only grow in the rank-one $\mathbf{y} \mathbf{y}^\top$ direction, by solving for the overlaps $\Phi = \phi \mathbf{y} \mathbf{y}^\top$ and $\hat{\Phi} = \hat{\phi} \mathbf{y} \mathbf{y}^\top$, we get

$$\phi = (1 + \delta + \hat{\phi})^{-1} + \delta^2 (1 + \delta + \hat{\phi})^{-2} \quad (46)$$

and similarly that

$$\hat{\phi} = -\gamma_0^2(\beta^{-1} + \phi)^{-2}. \quad (47)$$

In the same way, the saddle point equations for the source task \mathcal{T}_1 can be simplified in the source direction $\mathbf{y}\mathbf{y}^\top$, giving

$$\begin{aligned} \bar{\phi} &= (1 + \hat{\phi})^{-1} \\ \hat{\phi} &= -\bar{\gamma}_0^2(\beta^{-1} + \bar{\phi})^{-2}. \end{aligned} \quad (48)$$

Interestingly, here, when $\delta \rightarrow \infty$, since source and target tasks are uncorrelated, then $\phi = 1$, which means that the source kernel $\hat{\Phi}$ is the identity along the target direction \mathbf{y} as expected.

C.5.3 Same Data on Both Tasks

Another relevant case is the one where both source and target tasks share the same data and labels. If data are whitened, then

$$\mathbf{C}_{\mathcal{T}_1 \cup \mathcal{T}_2} = \begin{bmatrix} \mathbf{I} & \mathbf{I} \\ \mathbf{I} & \mathbf{I} \end{bmatrix}, \quad \langle \bar{\mathbf{h}}\bar{\mathbf{h}} \rangle = \begin{bmatrix} \mathbf{I} & \mathbf{I} \\ \mathbf{I} & \mathbf{I} \end{bmatrix} \begin{bmatrix} \mathbf{I} + \hat{\Phi} & \hat{\Phi} \\ \mathbf{0} & \mathbf{I} \end{bmatrix}^{-1} \quad (49)$$

which means

$$\langle \bar{\mathbf{h}}_2\bar{\mathbf{h}}_2 \rangle = -\left(\mathbf{I} + \hat{\Phi}\right)^{-1} \hat{\Phi} + \mathbf{I} = \left(\mathbf{I} + \hat{\Phi}\right)^{-1} \quad (50)$$

giving

$$\hat{\Phi} = \left[(1 + \delta)\mathbf{I} + \hat{\Phi}\right]^{-1} + \delta^2 \left[(1 + \delta)\mathbf{I} + \hat{\Phi}\right]^{-1} \left(\mathbf{I} + \hat{\Phi}\right)^{-1} \left[(1 + \delta)\mathbf{I} + \hat{\Phi}\right]^{-1}. \quad (51)$$

Again, we can solve for the overlaps, knowing that for \mathcal{T}_1

$$\bar{\phi} = (1 + \hat{\phi})^{-1} \quad (52)$$

$$\hat{\phi} = -\bar{\gamma}_0^2(\beta^{-1} + \bar{\phi})^{-2}. \quad (53)$$

For \mathcal{T}_2 we get

$$\phi = (1 + \delta + \hat{\phi})^{-1} + \delta^2 \bar{\phi} (1 + \delta + \hat{\phi})^{-2} \quad (54)$$

$$\hat{\phi} = -\gamma_0^2(\beta^{-1} + \phi)^{-2}. \quad (55)$$

Contrary to the previous uncorrelated case, here, when the elastic constraint $\delta \rightarrow \infty$, then $\phi = \bar{\phi}$ and the target kernel converges to the source kernel as expected.

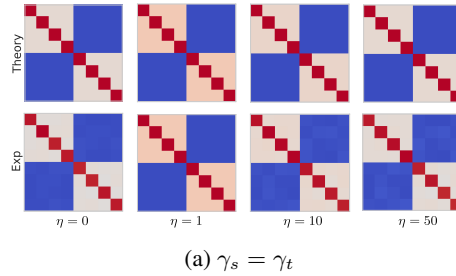


Figure 10: Kernels (theory vs experiments) as a function of the elastic constraint δ with the source task (\mathcal{T}_1). When $\gamma_s = \gamma_t$, there exists an optimal δ value for alignment with \mathcal{T}_2 , since in the target task you saw twice the data than in \mathcal{T}_1 .

C.5.4 Same Data, different labels

Suppose again that

$$\mathbf{C}_{\mathcal{T}_1 \cup \mathcal{T}_2} = \begin{bmatrix} \mathbf{I} & \mathbf{I} \\ \mathbf{I} & \mathbf{I} \end{bmatrix} \quad (56)$$

but that in principle, in this case,

From the saddle point equations for \mathcal{T}_1 , we know that

$$\bar{\Phi} = \mathbf{I} + (\bar{\phi} - 1) \mathbf{y}_1 \mathbf{y}_1^\top \quad (57)$$

and since the saddle point equations for \mathcal{T}_2 are

$$\begin{aligned} \Phi &= \left[(1 + \eta) \mathbf{I} + \hat{\Phi} \right]^{-1} + \eta^2 \left[(1 + \eta) \mathbf{I} + \hat{\Phi} \right]^{-1} (\mathbf{I} + (\bar{\phi} - 1) \mathbf{y}_1 \mathbf{y}_1^\top) \left[(1 + \eta) \mathbf{I} + \hat{\Phi} \right]^{-1} \\ \hat{\Phi} &= -\gamma_0^2 (\Phi)^{-1} \mathbf{y}_2 \mathbf{y}_2^\top (\Phi)^{-1} \end{aligned} \quad (58)$$

one realizes that the only non-trivial contributions to Φ comes from the span $\{\mathbf{y}_1, \mathbf{y}_2\}$, so in principle one can decompose

$$\Phi = a \mathbf{I} + b \mathbf{y}_1 \mathbf{y}_1^\top + c (\mathbf{y}_1 \mathbf{y}_2^\top + \mathbf{y}_2 \mathbf{y}_1^\top) + d \mathbf{y}_2 \mathbf{y}_2^\top \quad (59)$$

which means

$$\Phi = a \mathbf{I} + \begin{bmatrix} \mathbf{y}_1 & \mathbf{y}_2 \end{bmatrix} \begin{bmatrix} b & c \\ c & d \end{bmatrix} \begin{bmatrix} \mathbf{y}_1^\top \\ \mathbf{y}_2^\top \end{bmatrix} \quad (60)$$

from which

$$\Phi^{-1} = (a \mathbf{I} + \mathbf{u} \mathbf{C} \mathbf{u}^\top)^{-1} = a^{-1} \mathbf{I} - a^{-2} \mathbf{u} (\mathbf{C}^{-1} + a^{-1} \mathbf{u}^\top \mathbf{u})^{-1} \mathbf{u}^\top \quad (61)$$

and

$$\Phi^{-1} \mathbf{y}_2 = a^{-1} \mathbf{y}_2 - a^{-2} \mathbf{u} (\mathbf{C}^{-1} + a^{-1} \mathbf{u}^\top \mathbf{u})^{-1} \begin{bmatrix} \mathbf{y}_1^\top \mathbf{y}_2 \\ 1 \end{bmatrix} \quad (62)$$

being $\mathbf{y}_1^\top \mathbf{y}_2 = m$. It turns out, one can solve for $\{a, b, c, d\}$ self consistently and for different values of m .

D DMFT theory of transfer learning

In this section, we extend the derivation of [26] to include the effect of transfer learning in a two-layer network under gradient descent dynamics. As clarified in the main text in Eq. (1), given the mean-field parameterization we consider here, the gradient updates of our target network, whose first layer \mathbf{W} is constrained with an elastic force δ to the source weights $\bar{\mathbf{W}}$, are given by

$$\frac{d\mathbf{W}(t)}{dt} = -\frac{\gamma^2}{N} \sum_{\mu \in \mathcal{T}_2} \Delta_\mu(t) \mathbf{g}_\mu(t) \phi(\mathbf{h}_\mu(t))^\top - \lambda \mathbf{W}(t) - \delta (\mathbf{W}(t) - \bar{\mathbf{W}}) \quad (63)$$

$$\frac{d\mathbf{z}(t)}{dt} = -\frac{\gamma^2}{N} \sum_{\mu \in \mathcal{T}_2} \Delta_\mu(t) \phi(\mathbf{h}_\mu(t))^\top - \lambda \mathbf{z}(t) \quad (64)$$

by calling $\mathbf{g}_\mu = \frac{\partial f_\mu}{\partial \mathbf{h}_\mu}$ and $\Delta_\mu = -\frac{\partial \mathcal{L}}{\partial f_\mu}$. Now, by noticing that $\mathbf{h}_\mu(t) = \frac{1}{\sqrt{D}} \mathbf{W}(t) \mathbf{x}_\mu$ we get

$$\frac{d\mathbf{h}_\mu(t)}{dt} = -(\lambda + \delta) \mathbf{h}_\mu(t) + \delta \bar{\mathbf{h}}_\mu(t) + \gamma_0 \sum_{\nu} \Delta_\nu(t) \mathbf{g}_\nu(t) C_{\mu\nu}^{(2,2)} \quad (65)$$

where $C_{\mu\nu}^{(2,2)} = \frac{1}{D} \mathbf{x}_\mu \cdot \mathbf{x}_\nu$ with $\mu, \nu \in \mathcal{T}_2$. We notice that, when $\delta = 0$ and there is no transfer from \mathcal{T}_1 to \mathcal{T}_2 , the field dynamics is the same as [14]. Instead, as soon as $\delta > 0$, we get both contributions from the pre-activation fields of \mathcal{T}_1 and feature learning from \mathcal{T}_2 . We can do the same for the $\mathbf{z}_\mu(t)$ pre-gradient fields by noticing that $\mathbf{z} = \mathbf{w}(t)$ and then

$$\frac{d\mathbf{z}(t)}{dt} = \gamma_0 \sum_{\mu} \Delta_\mu(t) \phi(\mathbf{h}_\mu(t)). \quad (66)$$

As a consequence, the network predictor evolve as

$$\frac{df_\mu(t)}{dt} = \sum_{\nu \in \mathcal{T}_2} \left[\Phi_{\mu\nu}(t, t) + G_{\mu\nu}(t, t) C_{\mu\nu}^{(2,2)} \right] \Delta_\nu(t) - \lambda \kappa f_\mu(t) \quad (67)$$

having introduced the feature and gradient kernel definitions

$$\Phi_{\mu\nu}(t, s) = \frac{1}{N} \phi(\mathbf{h}_\mu(t)) \cdot \phi(\mathbf{h}_\nu(s)) \quad (68)$$

$$G_{\mu\nu}(t, s) = \frac{1}{N} \mathbf{g}_\mu(t) \cdot \mathbf{g}_\nu(s). \quad (69)$$

The second term in Eq. (67) depends on κ , which is the degree of homogeneity of the output

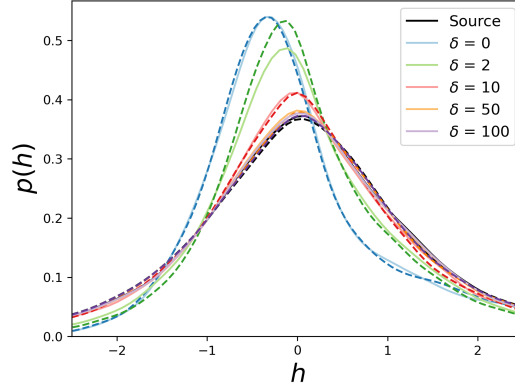


Figure 11: Preactivation distribution for different δ values. As δ becomes bigger, the target task distribution $p(\mathbf{h})$ recovers the source task distribution $p(\bar{\mathbf{h}})$. Full colored lines are from a $N = 5000$ ReLU NN under gradient descent. Corresponding dashed curves are from DMFT theory.

function, which we suppose $f(a\boldsymbol{\theta}) = a^\kappa f(\boldsymbol{\theta})$ as well as the activation $\phi(a\boldsymbol{\theta}) = a^\kappa \phi(\boldsymbol{\theta})$ (consistently with [26]). Now, to construct our mean field theory we should in principle compute the moment generating function

$$Z[\{\mathbf{j}_\mu, \mathbf{v}\}] = \left\langle \exp \left(\sum_{\mu} \mathbf{j}_\mu \cdot \boldsymbol{\xi}_\mu + \mathbf{v} \cdot \boldsymbol{\psi} \right) \right\rangle_{\boldsymbol{\theta}_0 = \text{Vec}\{\mathbf{W}(0), \mathbf{w}(0)\}} \quad (70)$$

whose average is taken over the random initialization of the fields $\boldsymbol{\xi}_\mu = \frac{1}{\sqrt{D}} \mathbf{W}(0) \mathbf{x}_\mu$ and $\boldsymbol{\psi} = \mathbf{w}(0)$, given the initialization of the weights as $\{W_{ij}, w_j\} \sim \mathcal{N}(0, 1)$. In this simple case of a two-layer NN this step is redundant, since by enforcing the fields $\boldsymbol{\xi}_\mu$ and $\boldsymbol{\psi}$ definitions through Dirac functions

$$1 = \int d\boldsymbol{\xi}_\mu \delta \left(\boldsymbol{\xi}_\mu - \frac{1}{\sqrt{D}} \mathbf{W}(0) \mathbf{x}_\mu \right) = \int \frac{d\boldsymbol{\xi}_\mu d\hat{\boldsymbol{\xi}}_\mu}{2\pi} \exp \left(i\hat{\boldsymbol{\xi}}_\mu \cdot \left(\boldsymbol{\xi}_\mu - \frac{1}{\sqrt{D}} \mathbf{W}(0) \mathbf{x}_\mu \right) \right) \quad (71)$$

$$1 = \int d\boldsymbol{\psi} \delta (\boldsymbol{\psi} - \mathbf{w}(0)) = \int \frac{d\boldsymbol{\psi} d\hat{\boldsymbol{\psi}}}{2\pi} \exp \left(i\hat{\boldsymbol{\psi}} \cdot (\boldsymbol{\psi} - \mathbf{w}(0)) \right) \quad (72)$$

we realize that, because the field have no time dependency, it is enough to just keep track of the feature and gradient kernels values at each time t , i.e. $\Phi_{\mu\nu}(t, t)$, $G_{\mu\nu}(t, t)$ and not their correlation across times. In this case, by enforcing the kernel definitions of Eq. (68) in the same way as Eq. (71), in the infinite width limit $N \rightarrow \infty$ we get a MGF of the form $Z = \int d\Phi d\hat{\Phi} dG d\hat{G} \exp \left(NS \left[\Phi, \hat{\Phi}, G, \hat{G} \right] \right)$, and because everything is factorized over the N neurons and the kernels concentrate, we get

$$\begin{aligned} \Phi_{\mu\nu}(t, t) &= \langle \phi(h_\mu(t)) \phi(h_\nu(t)) \rangle, & \hat{\Phi}_{\mu\nu}(t, t) &= 0 \\ G_{\mu\nu}(t, t) &= \langle g_\mu(t) g_\nu(t) \rangle, & \hat{G}_{\mu\nu}(t, t) &= 0 \end{aligned} \quad (73)$$

which are averages over the stochastic processes

$$\begin{aligned}
h_\mu(t) &= e^{-(\lambda+\delta)t} \xi_\mu + \frac{\delta}{\lambda+\delta} \left(1 - e^{-(\lambda+\delta)t}\right) \bar{h}_\mu \\
&+ \gamma_0 \int_0^t ds e^{-(\lambda+\delta)(t-s)} \sum_\nu \Delta_\nu(s) g_\nu(s) C_{\mu\nu}^{(2,2)} \\
z(t) &= e^{-\lambda t} \psi + \gamma_0 \int_0^t e^{-\lambda(t-s)} \sum_\mu \Delta_\mu(s) \phi(h_\mu(s)) \\
g_\mu(t) &= \dot{\phi}(h_\mu(t)) z(t).
\end{aligned} \tag{74}$$

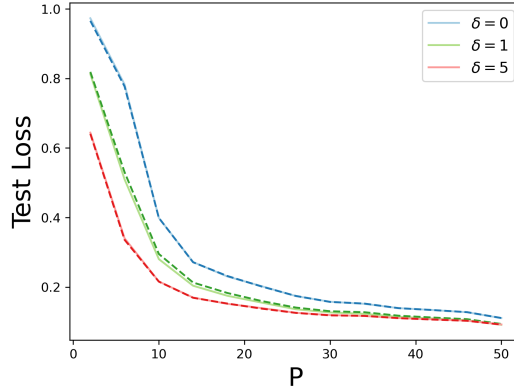


Figure 12: Test loss vs P_2 for different δ . Transfer learning is much more effective when sample size P_2 is small. Source task: $P_1 = 1000$ for $\{0, 5\}$ classes of Fashion-MNIST and $\bar{\gamma}_0 = 1.0$. Target: P_2 for $\{0, 9\}$ classes of Fashion-MNIST.

D.1 CNN extension

It is easy to extend the DMFT field equations for a two-layer CNN. In this case, the network definition involves convolution over a set of spatial indices $a, b \in \mathcal{S}^0$

$$h_{\mu ia} = \frac{1}{\sqrt{D}} \sum_{j=1}^D \sum_{b \in \mathcal{S}^0} W_{ijb} x_{\mu, j, a+b} \tag{75}$$

$$f_\mu = \frac{1}{\gamma_0 N} \sum_{i=1}^N \sum_a w_{ia} \phi(h_{\mu ia}). \tag{76}$$

In our notation a is the spatial displacement from the center of the filter at each layer where $b \in \mathcal{S}^\ell$ is the spatial relative field at layer ℓ . The gradient signal is now defined as

$$\mathbf{g}_{\mu, a} = \gamma_0 N \sum_b \frac{\partial f}{\partial \mathbf{h}_{\mu, b}^{\ell+1}} \tag{77}$$

while the weight dynamics per filter is

$$\frac{d}{dt} \mathbf{W}_b(t) = \frac{\gamma_0}{\sqrt{N}} \sum_{\mu, a} \Delta_\mu \mathbf{g}_{\mu, a} \phi(\mathbf{h}_{\mu, a+b})^\top - \lambda \mathbf{W}_b(t) - \delta (\mathbf{W}_b(t) - \bar{\mathbf{W}}_b) \tag{78}$$

Given that, the stochastic dynamics for the pre-activation and pre-gradient signals becomes

$$\begin{aligned} \mathbf{h}_{\mu,a}(t) &= e^{-(\lambda+\delta)t} \boldsymbol{\xi}_{\mu,a}(t) + \frac{\delta}{\lambda+\delta} (1 - e^{-(\lambda+\delta)t}) \bar{\mathbf{h}}_{\mu,a} \\ &+ \gamma_0 \int_0^t dt' e^{-(\lambda+\delta)(t-t')} \sum_{\nu,b,c} \Delta_\nu(t') C_{\mu\nu,a+b,a+c}^{(2,2)}(t,t') \mathbf{g}_{\nu,c}^{\ell+1}(t') \\ \mathbf{z}_{\mu,a}(t) &= e^{-\lambda t} \boldsymbol{\psi}_{\mu,a}(t) + \gamma_0 \int_0^t dt' e^{-\lambda(t-t')} \sum_{\nu,b,c} \Delta_\nu(t') G_{\mu\nu,a-b,c-b}(t,t') \phi(\mathbf{h}_{\nu,c}) \end{aligned}$$

where again $\boldsymbol{\xi}_{\mu,a}^{\ell+1}(t) = \frac{1}{\sqrt{N}} \mathbf{W}^\ell(0) \phi(\mathbf{h}_{\mu,a}^\ell(t))$ and $\boldsymbol{\psi}_{\mu,a}^\ell(t) = \frac{1}{\sqrt{N}} \mathbf{W}^\ell(0) g_{\mu,a}^{\ell+1}(t)$ from the initial conditions.

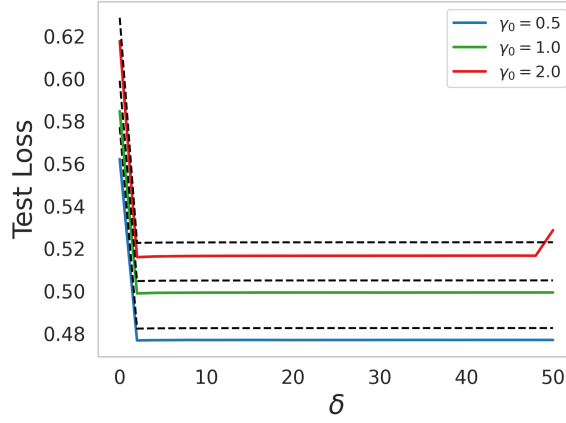


Figure 13: Test loss of a two layer CNN vs δ for different feature learning parameters γ_0 . Source task is animate $\{2, 3, 4\}$ vs inanimate $\{0, 1, 8\}$ classes from CIFAR10 with $P_1 = 1200$ and $\tilde{\gamma}_0 = 1.0$, target task is animate $\{2, 3, 5\}$ vs inanimate $\{0, 1, 9\}$ classes from CIFAR10 with $P_2 = 200$.